into the negative, weak, moderate, and strong groups was 62, 16, 55, and 87, respectively. From these results, we judged that NS expression showed bimodal distribution and used a 10% threshold for NS positivity between negative and positive groups.

NS protein was frequently detected in the nucleus of breast cancer cells. Although strong immunoreaction was observed in both the nucleoli and nucleoplasm of cancer cells (Figure 1A), nuclear immunoreaction of NS in some cases was limited to the nucleoli of cancer cells (Figure 1B). Such cells were also judged as positive for NS immunoreactivity. Cytoplasmic staining was not observed. These findings are consistent with those of previous reports [6,17,19]. We found that 78 (35.5%) or 142 (64.5%) patients had NS-negative or NS-positive tumors, respectively (Figure 1C). Unremarkable mammary glands showed nuclear NS immunoreactivity in almost all luminal epithelial cells (Figure 1D).

Tumors with NS positivity showed a higher frequency of ER positivity, HER2 positivity, and p53 positivity ($P = 0.050$, $P = 0.021$, and $P = 0.031$, respectively), whereas NS expression status was not correlated with tumor size, lymph node metastasis, distant metastasis, tumor nuclear grade, or PgR positivity. NS expression was detected at 50% or more in all histological types studied except tubular carcinoma (20%), and the positive rate was 100% (6 of 6) in mucinous carcinoma. Patients with NS-positive tumors showed significantly shorter DFS time than those with NS-negative tumors ($P = 0.020$, Figure 2).

Prognostic implication of the NS and p53 combination status for the entire patient cohort

Since it has been reported that physical and functional interaction between NS and p53 appear to be essential for self-renewal, cell cycle regulation, cell proliferation, and apoptosis [7], we next examined the prognostic implication of the combination status of NS and p53 for the entire patient cohort. We found that 143 (65%) and 77 (35%) patients had p53-negative and p53-positive tumors, respectively. The patients with p53-positive tumors showed significantly shorter DFS time than those with p53-negative tumors ($P = 0.006$, Figure 3A).

A striking stratification of relapse risk was identified when three different combinations of NS and p53 status were evaluated: 57 cases with a combination of NS-positive/p53-positive tumors (unfavorable group); 105 cases comprising 20 NS-negative/p53-positive tumors and 85 NS-positive/p53-negative tumors (intermediate group); and 58 cases with NS-negative/p53-negative tumors (favorable group). The unfavorable group had a 5-year DFS rate of 55%, compared with 75% in the intermediate group and 86% in the favorable group (Figure 3B). The unfavorable group had significantly shorter DFS time than the intermediate and favorable groups (log-rank test $P = 0.034$ and $P = 0.0007$, respectively).

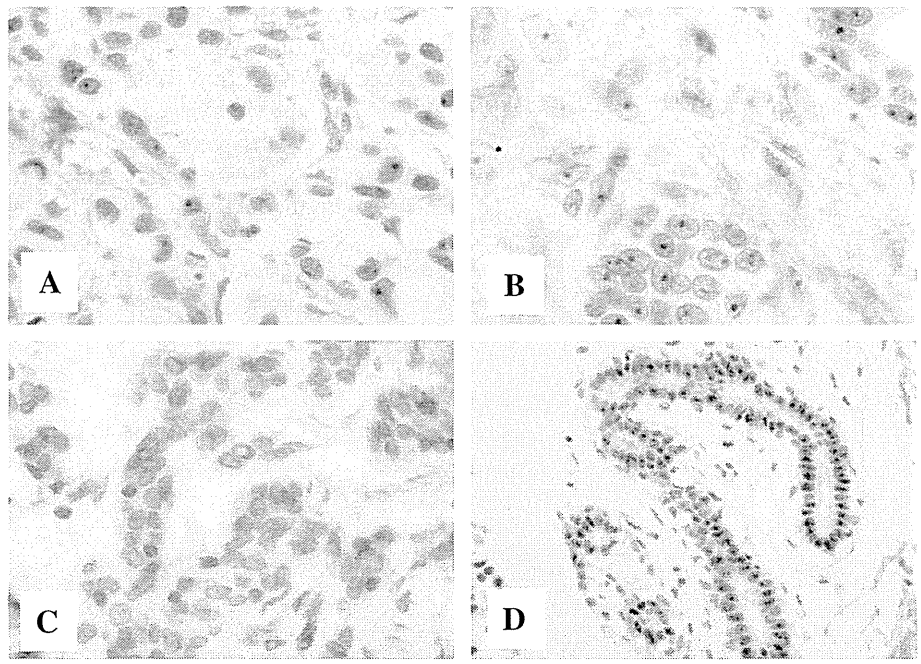

Figure 1 Nucleostemin (NS) expression in human breast cancer tissues. A. A NS-positive tumor. Almost all cancer cells show NS immunoreactivity in both nucleoli and nucleoplasm. **B.** Another NS-positive tumor, NS immunoreactivity is limited to nucleoli in nuclei of cancer cells. Such cancer cells are also judged as NS-positive. This case was also classified as NS-positive. **C.** A NS-negative tumor. **D.** An unremarkable mammary gland shows nuclear NS immunoreactivity in almost all luminal epithelial cells.

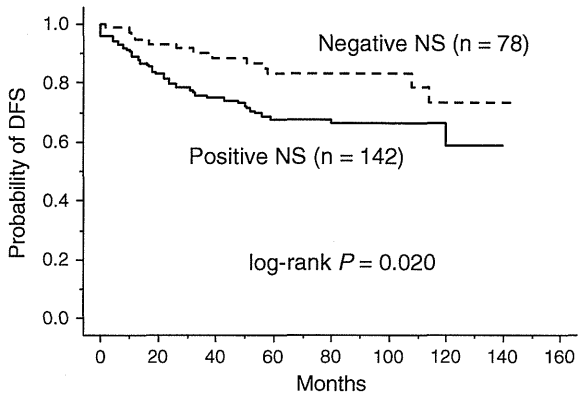

Figure 2 Prognostic impact of NS status in the patients with primary breast cancer. This figure shows disease-free survival (DFS) curves for the 142 patients with NS-positive tumors and for the 78 patients with NS-negative tumors. These two curves differ significantly ($P = 0.020$).

Prognostic implication of NS among the three biological subtypes of breast tumors

Currently, treatment strategies differ between the biological subtypes of breast tumors; therefore, we examined the prognostic implication of NS among three groups of patients divided based on their biological subtype: 154 patients with luminal-type tumors (HR-positive); 22 patients with HER2-type tumors (HER2-positive and HR-negative); and 44 patients with triple-negative tumors (HR and HER2-negative). Eight patients with HR-positive and HER2-positive tumors were included and analyzed as luminal-type patients.

Among the patients with luminal-type tumors, patients with NS-positive tumors showed a significantly shorter DFS time than those with NS-negative tumors ($P = 0.033$, Figure 4A). Among the patients with HER2-positive tumors, patients with NS-positive tumors had a 5-year DFS rate of 28% compared with 100% in patients with NS-negative tumors (Figure 4B). However, the *P*-value was not calculated because there was no relapse

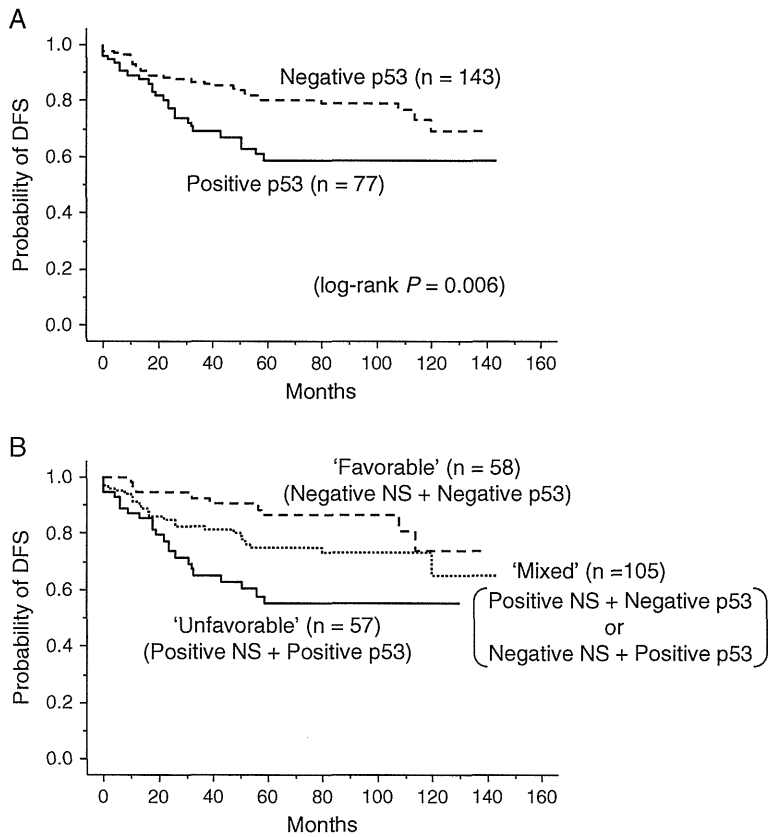

Figure 3 Prognostic impact of the combination status of NS and p53 in the patients with primary breast cancer. A. Disease-free survival (DFS) curves for the 77 patients with p53-positive tumors and for the 143 patients with p53-negative tumors. These two curves differ significantly ($P = 0.006$). **B.** This figure shows three disease-free survival (DFS) curves: for the 57 patients with NS-positive and p53-positive tumors ('unfavorable group'), for 105 patients comprising 20 NS-negative and p53-positive tumors and 85 NS-positive and p53-negative tumors ('intermediate' group), and for 58 patients with NS-negative and p53-negative tumors ('favorable' group). The unfavorable group has significantly shorter DFS time than the intermediate group or the favorable group (log-rank test $P = 0.034$ and $P = 0.0007$, respectively).

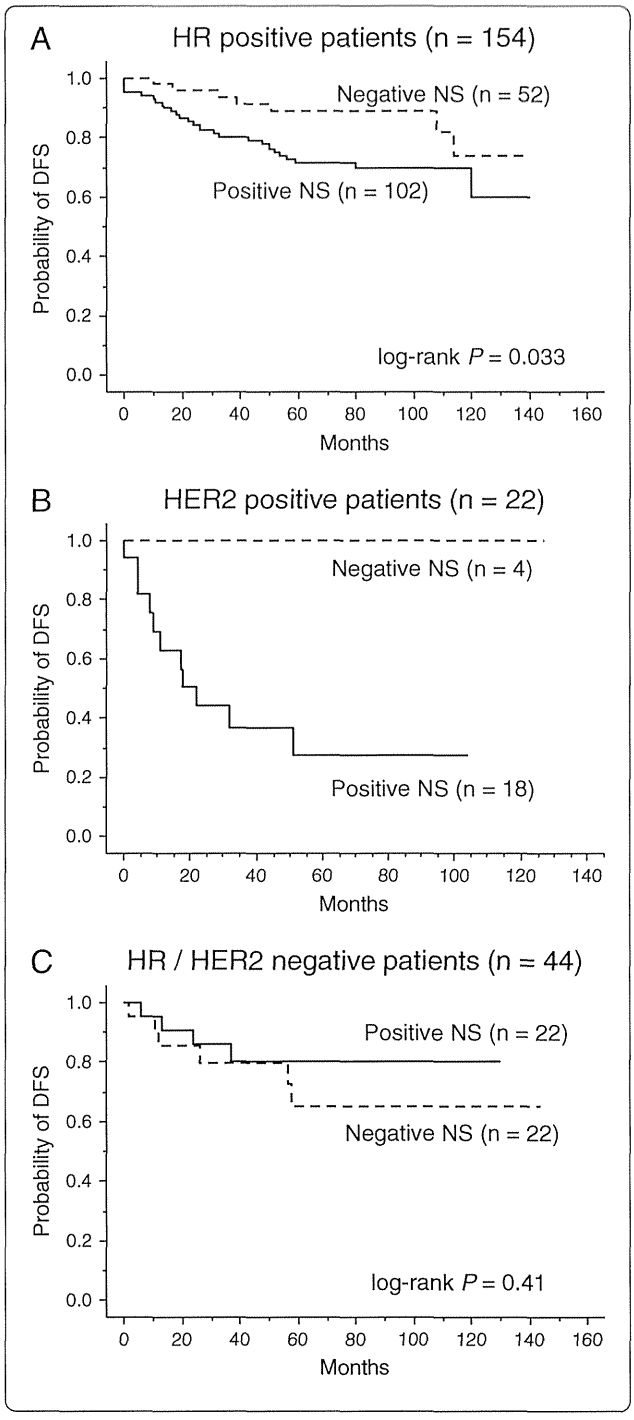

Figure 4 Prognostic impact of NS status in the three subgroups of the different biological subtype tumors: luminal-type tumors, HER2-type tumors, and triple-negative tumors. **A.** Subgroup analysis of the 154 patients with luminal-type tumors (HR-positive tumors). Two disease-free survival (DFS) curves, that for the 102 patients with NS-positive tumors and that for the 52 patients with NS negative tumors, differ significantly ($P = 0.033$). **B.** Subgroup analysis of the 22 patients with HER2-type tumors (HER2-positive and HR-negative tumors). In two disease-free survival (DFS) curves, that for the 18 patients with NS-positive tumors and that for the 4 patients with NS-negative tumors, five-year DFS rates differ largely (100% vs 28%). *P*-value was not available because there was no relapse in the patients with NS-negative tumors. **C.** Subgroup analysis of the 44 patients with triple-negative tumors (HR and HER2 negative tumors). The two curves do not differ significantly ($P = 0.41$).

in the four patients with NS-negative tumors. Among the patients with triple-negative tumors, there was no difference between the survival curves for patients with NS-positive tumors and those with NS-negative tumors ($P = 0.41$, Figure 4C).

Multivariate analysis of prognostic factors and evaluation of NS

Univariate analysis showed that HR, HER2, nuclear grade, tumor size, nodal status, distant metastasis, and NS expression were significantly correlated with DFS. When multivariate analysis was performed using these seven factors, NS expression status was selected as an independent prognostic factor ($P = 0.036$), together with nuclear grade, tumor size, lymph node status, and distant metastatic status ($P = 0.0008$, 0.0007, 0.0038 and <0.0001, respectively; Table 2).

Discussion

In the present cohort, we found that the NS protein expression status was positively correlated with both ER and HER2 status and was a powerful prognostic factor. Patients with NS-positive breast tumors had a significantly shorter DFS time than those with NS-negative tumors ($P = 0.020$, Figure 2), and multivariate analysis for DFS showed that NS positivity had an independent impact as a prognostic indicator among breast cancer patients ($P = 0.036$, Table 2). To our knowledge, this is the first report to show the clinical implication of NS protein expression in invasive breast cancers.

Although several studies have shown the important roles of NS in the pathogenesis of various cancer types [8-13] as well as the maintenance of cancer stem cells [14,15], no direct evidence is yet available to support that NS is a marker of cancer stem cells. Currently, molecules such as CD44, CD133, ALDH1, and CXCR4 have been found to be potential markers of cancer stem cells [20-25]. Furthermore, the expression of these stem cell markers has been shown to be a poor prognostic

Table 2 Prognostic impacts of clinicopathological variables computed by Cox's univariate and multivariate analyses in patients with primary breast cancer

		Univariate			Multivariate		
		Hazard ratio	(95% CI)	P-value	Hazard ratio	(95%CI)	P-value
Disease free survival							
Nucleostemin	Negative	1		0.023	1		0.036
	Positive	2.06	(1.11-3.84)		2.13	(1.05-4.33)	
Hormone-receptor	Positive	1		0.045	1		0.46
	Negative	1.73	(1.01-2.95)		0.78	(0.39-1.52)	
HER2	Negative	1		0.0005	1		0.17
	Positive	2.91	(1.59-5.34)		1.65	(0.80-3.41)	
Nuclear grade	1, 2	1		<0.0001	1		0.0008
	3	3.30	(1.94-5.64)		2.97	(1.57-5.61)	
Tumor size	≦5.0 cm	1		<0.0001	1		0.0007
	>5.0 cm	6.89	(3.97-11.9)		2.99	(1.59-5.66)	
Nodal status	Negative	1		<0.0001	1		0.0038
	Positive	4.51	(2.45-8.31)		2.73	(1.38-5.38)	
Distant metastasis	Negative	1		<0.0001	1		<0.0001
	Positive	71.6	(26.1-196.5)		62.3	(15.5-251.1)	

Abbreviation: 95% CI 95% confidence interval.

indicator in several human cancer types [24,26-30]. Based on these observations, our results show that high NS expression is a powerful indicator of poor outcome, consistent with the idea that NS may be a breast cancer stem cell marker.

The limitations of the present study included the retrospective analyses and the heterogeneity of adjuvant treatments. Therefore, one should pay careful attention when interpreting these results. Further studies using a uniformly treated patient cohort are required to clarify the role of NS in breast cancer stem cells.

We found that the patient group with tumors coexpressing NS and p53 had shorter DFS times than the patient group with tumors negative for either NS or p53. GTP binding modulates the movement of NS from the nucleoli to the nucleoplasm; NS then binds p53 at its N-terminal basic domain, which results in the suppression of p53 function [6,7]. Because prolongation of the half-life of most of the mutated p53 protein induces its nuclear accumulation, it is generally believed that the p53 pathway does not fully function in tumors with high p53 nuclear immunoreactivity [31-33]. This evidence leads to the assumption that p53 function would be profoundly suppressed in tumors coexpressing NS and p53. Our results show the validity of this concept and that functional crosstalk between NS and p53 may also occur *in vivo*.

Currently, we cannot explain the correlation between NS expression and p53 expression. Although several studies have shown that NS modulates the expression of wild-type p53 [34,35], the role of NS in breast cancers with mutant p53 has not yet been evaluated. Further research is needed to elucidate the correlation.

We found that the NS expression status was positively correlated with both ER and HER2 status and also found a significant prognostic implication of NS expression for patients with luminal-type tumors and those with HER2-type tumors, except for those with triple-negative tumors. NS was first identified as a gene upregulated in MCF-7 cells upon 17β-estradiol treatment [36]; therefore, our inclusion of subgroup analysis among patients with luminal-type tumors was reasonable. To our knowledge, this is the first report to demonstrate the possible association between NS and HER2. Zhang G et al. showed that NS is required for the expression of EGF and EGFR in an esophageal squamous carcinoma cell line [13]. Presumably, NS is required for the expression of HER2 in a manner similar to that for EGFR. We found no survival impact of the NS expression status among patients with triple-negative tumors, who show higher rates of mutated p53 than patients with luminal-type or HER2-type tumors [37]. NS can function in the presence of wide-type p53 [7]; therefore, the expression status of NS may have survival impact only for the luminal-type and HER2-type tumors.

Conclusions

In summary, our results indicate that the expression status of NS, abundant in stem cells, is a prognostic indicator in breast cancer patients, especially for those with

luminal-type or HER2-type tumors, and that the co-expression of NS and p53 correlates with poorer prognostic outcomes. Examination of NS expression may be useful for the stratification and management of breast cancer patients in future daily practice.

Competing interests
The authors declare no conflicts of interest.

Authors' contributions
TK and HT conceived of the study, performed experiments, analyzed data and wrote the manuscript. TM, TY, and JY provided samples, collected clinical and pathological data. KM, KT, YF, and ST participated in designing the study and revising the manuscript. HT participated in the overall design and study coordination and finalized the draft of the manuscript. All authors read and approved the final manuscript.

Acknowledgments
This work was supported in part by the Foundation for Promotion of Defense Medicine and by the Cancer Research and Development Fund from the National Cancer Center, Japan.

Author details
[1]Department of Basic Pathology, National Defense Medical College, 3-2 Namiki, Tokorozawa, Saitama 359-8513, Japan. [2]Department of Medical Oncology, Cancer Institute Hospital, 3-8-31 Ariake, Koto-ku, Tokyo 135-8550, Japan. [3]Division of Cancer Stem Cell, National Cancer Center Research Institute, Tsukiji, Chuo-ku, Tokyo 104-0045, Japan. [4]Department of Breast Oncology and Medical Oncology, National Cancer Center Hospital, 5-1-1 Tsukiji, Chuo-ku, Tokyo 104-0045, Japan. [5]Department of Surgery, National Defense Medical College, 3-2 Namiki, Tokorozawa, Saitama 359-8513, Japan. [6]Department of Pathology and Clinical Laboratories, National Cancer Center Hospital, 5-1-1 Tsukiji, Chuo-ku, Tokyo 104-0045, Japan.

Received: 19 October 2013 Accepted: 11 March 2014
Published: 21 March 2014

References
1. O'Shaughnessy J: **Extending survival with chemotherapy in metastatic breast cancer.** *Oncologist* 2005, **10**(Suppl 3):20–29.
2. Pagani O, Senkus E, Wood W, Colleoni M, Cufer T, Kyriakides S, Costa A, Winer EP, Cardoso F: **International guidelines for management of metastatic breast cancer: can metastatic breast cancer be cured?** *J Natl Cancer Inst* 2010, **102**(7):456–463.
3. Clarke MF, Fuller M: **Stem cells and cancer: two faces of eve.** *Cell* 2006, **124**(6):1111–1115.
4. Reya T, Morrison SJ, Clarke MF, Weissman IL: **Stem cells, cancer, and cancer stem cells.** *Nature* 2001, **414**(6859):105–111.
5. Dean M, Fojo T, Bates S: **Tumour stem cells and drug resistance.** *Nat Rev Cancer* 2005, **5**(4):275–284.
6. Tsai RY, McKay RD: **A nucleolar mechanism controlling cell proliferation in stem cells and cancer cells.** *Genes Dev* 2002, **16**(23):2991–3003.
7. Bernardi R, Pandolfi PP: **The nucleolus: at the stem of immortality.** *Nat Med* 2003, **9**(1):24–25.
8. Ye F, Zhou C, Cheng Q, Shen J, Chen H: **Stem-cell-abundant proteins Nanog, Nucleostemin and Musashi1 are highly expressed in malignant cervical epithelial cells.** *BMC Cancer* 2008, **8**:108.
9. Fan Y, Liu Z, Zhao S, Lou F, Nilsson S, Ekman P, Xu D, Fang X: **Nucleostemin mRNA is expressed in both normal and malignant renal tissues.** *Br J Cancer* 2006, **94**(11):1658–1662.
10. Liu RL, Zhang ZH, Zhao WM, Wang M, Qi SY, Li J, Zhang Y, Li SZ, Xu Y: **Expression of nucleostemin in prostate cancer and its effect on the proliferation of PC-3 cells.** *Chin Med J (Engl)* 2008, **121**(4):299–304.
11. Cada Z, Boucek J, Dvorankova B, Chovanec M, Plzak J, Kodets R, Betka J, Pinot GL, Gabius HJ, Smetana K Jr: **Nucleostemin expression in squamous cell carcinoma of the head and neck.** *Anticancer Res* 2007, **27**(5A):3279–3284.
12. Malakootian M, Mowla SJ, Saberi H, Asadi MH, Atlasi Y, Shafaroudi AM: **Differential expression of nucleostemin, a stem cell marker, and its variants in different types of brain tumors.** *Mol Carcinog* 2010, **49**(9):818–825.
13. Zhang G, Zhang Q, Yin L, Li S, Cheng K, Zhang Y, Xu H, Wu W: **Expression of nucleostemin, epidermal growth factor and epidermal growth factor receptor in human esophageal squamous cell carcinoma tissues.** *J Cancer Res Clin Oncol* 2010, **136**(4):587–594.
14. Tamase A, Muraguchi T, Naka K, Tanaka S, Kinoshita M, Hoshii T, Ohmura M, Shugo H, Ooshio T, Nakada M, Sawamoto K, Onodera M, Matsumoto K, Oshima M, Asano M, Saya H, Okano H, Suda T, Hamada J, Hirao A: **Identification of tumor-initiating cells in a highly aggressive brain tumor using promoter activity of nucleostemin.** *Proc Natl Acad Sci U S A* 2009, **106**(40):17163–17168.
15. Okamoto N, Yasukawa M, Nguyen C, Kasim V, Maida Y, Possemato R, Shibata T, Ligon KL, Fukami K, Hahn WC, Masutomi K: **Maintenance of tumor initiating cells of defined genetic composition by nucleostemin.** *Proc Natl Acad Sci U S A* 2011, **108**(51):20388–20393.
16. Kobayashi T, Tsuda H, Moriya T, Yamasaki T, Kikuchi R, Ueda S, Omata J, Yamamoto J, Matsubara O: **Expression pattern of stromal cell-derived factor-1 chemokine in invasive breast cancer is correlated with estrogen receptor status and patient prognosis.** *Breast Cancer Res Treat* 2010, **123**(3):733–745.
17. Nakajima TE, Yoshida H, Okamoto N, Nagashima K, Taniguchi H, Yamada Y, Shimoda T, Masutomi K: **Nucleostemin and TWIST as predictive markers for recurrence after neoadjuvant chemotherapy for esophageal carcinoma.** *Cancer Sci* 2012, **103**(2):233–238.
18. Wolff AC, Hammond ME, Schwartz JN, Hagerty KL, Allred DC, Cote RJ, Dowsett M, Fitzgibbons PL, Hanna WM, Langer A, McShane LM, Paik S, Pegram MD, Perez EA, Press MF, Rhodes A, Sturgeon C, Taube SE, Tubbs R, Vance GH, van de Vijver M, Wheeler TM, Hayes DF: **American Society of Clinical Oncology/College of American Pathologists guideline recommendations for human epidermal growth factor receptor 2 testing in breast cancer.** *J Clin Oncol* 2007, **25**(1):118–145.
19. Yoshida R, Fujimoto T, Kudoh S, Nagata M, Nakayama H, Shinohara M, Ito T: **Nucleostemin affects the proliferation but not differentiation of oral squamous cell carcinoma cells.** *Cancer Sci* 2011, **102**(7):1418–1423.
20. Al-Hajj M, Wicha MS, Benito-Hernandez A, Morrison SJ, Clarke MF: **Prospective identification of tumorigenic breast cancer cells.** *Proc Natl Acad Sci U S A* 2003, **100**(7):3983–3988.
21. O'Brien CA, Pollett A, Gallinger S, Dick JE: **A human colon cancer cell capable of initiating tumour growth in immunodeficient mice.** *Nature* 2007, **445**(7123):106–110.
22. Ricci-Vitiani L, Lombardi DG, Pilozzi E, Biffoni M, Todaro M, Peschle C, De Maria R: **Identification and expansion of human colon-cancer-initiating cells.** *Nature* 2007, **445**(7123):111–115.
23. Singh SK, Hawkins C, Clarke ID, Squire JA, Bayani J, Hide T, Henkelman RM, Cusimano MD, Dirks PB: **Identification of human brain tumour initiating cells.** *Nature* 2004, **432**(7015):396–401.
24. Ginestier C, Hur MH, Charafe-Jauffret E, Monville F, Dutcher J, Brown M, Jacquemier J, Viens P, Kleer CG, Liu S, Schott A, Hayes D, Birnbaum D, Wicha MS, Dontu G: **ALDH1 is a marker of normal and malignant human mammary stem cells and a predictor of poor clinical outcome.** *Cell Stem Cell* 2007, **1**(5):555–567.
25. Hermann PC, Huber SL, Herrler T, Aicher A, Ellwart JW, Guba M, Bruns CJ, Heeschen C: **Distinct populations of cancer stem cells determine tumor growth and metastatic activity in human pancreatic cancer.** *Cell Stem Cell* 2007, **1**(3):313–323.
26. Joensuu H, Klemi PJ, Toikkanen S, Jalkanen S: **Glycoprotein CD44 expression and its association with survival in breast cancer.** *Am J Pathol* 1993, **143**(3):867–874.
27. Tempfer C, Losch A, Heinzl H, Hausler G, Hanzal E, Kolbl H, Breitenecker G, Kainz C: **Prognostic value of immunohistochemically detected CD44 isoforms CD44v5, CD44v6 and CD44v7-8 in human breast cancer.** *Eur J Cancer* 1996, **32A**(11):2023–2025.
28. Horst D, Kriegl L, Engel J, Kirchner T, Jung A: **CD133 expression is an independent prognostic marker for low survival in colorectal cancer.** *Br J Cancer* 2008, **99**(8):1285–1289.
29. Maeda S, Shinchi H, Kurahara H, Mataki Y, Maemura K, Sato M, Natsugoe S, Aikou T, Takao S: **CD133 expression is correlated with lymph node metastasis and vascular endothelial growth factor-C expression in pancreatic cancer.** *Br J Cancer* 2008, **98**(8):1389–1397.
30. Marechal R, Demetter P, Nagy N, Berton A, Decaestecker C, Polus M, Closset J, Deviere J, Salmon I, Van Laethem JL: **High expression of CXCR4 may predict poor survival in resected pancreatic adenocarcinoma.** *Br J Cancer* 2009, **100**(9):1444–1451.

31. Davidoff AM, Herndon JE 2nd, Glover NS, Kerns BJ, Pence JC, Iglehart JD, Marks JR: **Relation between p53 overexpression and established prognostic factors in breast cancer.** *Surgery* 1991, **110**(2):259–264.
32. Bartek J, Bartkova J, Lukas J, Staskova Z, Vojtesek B, Lane DP: **Immunohistochemical analysis of the p53 oncoprotein on paraffin sections using a series of novel monoclonal antibodies.** *J Pathol* 1993, **169**(1):27–34.
33. Soussi T, Legros Y, Lubin R, Ory K, Schlichtholz B: **Multifactorial analysis of p53 alteration in human cancer: a review.** *Int J Cancer* 1994, **57**(1):1–9.
34. Ma H, Pederson T: **Depletion of the nucleolar protein nucleostemin causes G1 cell cycle arrest via the p53 pathway.** *Mol Biol Cell* 2007, **18**(7):2630–2635.
35. Dai MS, Sun XX, Lu H: **Aberrant expression of nucleostemin activates p53 and induces cell cycle arrest via inhibition of MDM2.** *Mol Cell Biol* 2008, **28**(13):4365–4376.
36. Charpentier AH, Bednarek AK, Daniel RL, Hawkins KA, Laflin KJ, Gaddis S, MacLeod MC, Aldaz CM: **Effects of estrogen on global gene expression: identification of novel targets of estrogen action.** *Cancer Res* 2000, **60**(21):5977–5983.
37. Sorlie T, Perou CM, Tibshirani R, Aas T, Geisler S, Johnsen H, Hastie T, Eisen MB, van de Rijn M, Jeffrey SS, Thorsen T, Quist H, Matese JC, Brown PO, Botstein D, Eystein Lonning P, Borresen-Dale AL: **Gene expression patterns of breast carcinomas distinguish tumor subclasses with clinical implications.** *Proc Natl Acad Sci U S A* 2001, **98**(19):10869–10874.

doi:10.1186/1471-2407-14-215
Cite this article as: Kobayashi *et al.*: Nucleostemin expression in invasive breast cancer. *BMC Cancer* 2014 **14**:215.

MCB
Journals.ASM.org

Involvement of Telomerase Reverse Transcriptase in Heterochromatin Maintenance

Yoshiko Maida,[a] Mami Yasukawa,[a] Naoko Okamoto,[a,b] Seii Ohka,[a] Keita Kinoshita,[a] Yasushi Totoki,[c] Takashi K. Ito,[d] Tohru Minamino,[e] Hiromi Nakamura,[c] Satoko Yamaguchi,[a] Tatsuhiro Shibata,[c] Kenkichi Masutomi[a,f]

Division of Cancer Stem Cell, National Cancer Center Research Institute, Tokyo, Japan[a]; Laboratory of Genome and Biosignal, Tokyo University of Pharmacy and Life Science, Tokyo, Japan[b]; Division of Cancer Genomics, National Cancer Center Research Institute, Tokyo, Japan[c]; Department of Cardiovascular Science and Medicine, Chiba University, Chiba, Japan[d]; Department of Cardiovascular Biology and Medicine, Niigata University Graduate School of Medical and Dental Sciences, Niigata, Japan[e]; PREST, Japan Science and Technology Agency, Saitama, Japan[f]

In the fission yeast *Schizosaccharomyces pombe*, centromeric heterochromatin is maintained by an RNA-directed RNA polymerase complex (RDRC) and the RNA-induced transcriptional silencing (RITS) complex in a manner that depends on the generation of short interfering RNA. In association with the telomerase RNA component (TERC), the telomerase reverse transcriptase (TERT) forms telomerase and counteracts telomere attrition, and without TERC, TERT has been implicated in the regulation of heterochromatin at locations distinct from telomeres. Here, we describe a complex composed of human TERT (hTERT), Brahma-related gene 1 (BRG1), and nucleostemin (NS) that contributes to heterochromatin maintenance at centromeres and transposons. This complex produced double-stranded RNAs homologous to centromeric alpha-satellite (*alphoid*) repeat elements and transposons that were processed into small interfering RNAs targeted to these heterochromatic regions. These small interfering RNAs promoted heterochromatin assembly and mitotic progression in a manner dependent on the RNA interference machinery. These observations implicate the hTERT/BRG1/NS (TBN) complex in heterochromatin assembly at particular sites in the mammalian genome.

Telomeres and centromeres are both tightly condensed heterochromatic areas within the genome, and the maintenance of heterochromatin is important for overall genome stability. In *Schizosaccharomyces pombe*, heterochromatin near centromeres is maintained by the RNA-directed RNA polymerase complex (RDRC) and the RNA-induced transcriptional silencing (RITS) complex (1, 2). Specifically, inhibition of RNA-dependent RNA polymerase (RdRP) activity leads to loss of small interfering RNAs (siRNAs) that are associated with the RITS complex and correlates with loss of transcriptional silencing and heterochromatin at centromeres (3). In addition, when RdRP activity is inhibited, siRNAs that are usually associated with the RITS complex are lost (4). These observations implicate RdRPs as a component of a loop coupling heterochromatin assembly to siRNA production.

In *Caenorhabditis elegans*, the Argonaute CSR-1, the RdRP EGO-1, and the Dicer-related helicase DRH-3 localize to chromosomes and are required for proper chromosome segregation, and in the absence of these factors, chromosomes fail to properly align in mitotic phase (5, 6). Moreover, a conserved germ line-specific nucleotidyltransferase, CDE-1, localizes specifically to mitotic chromosomes in embryos in a manner that requires the RdRP EGO-1, which physically interacts with CDE-1, and the Argonaute protein CSR-1 (5, 6). Although it is clear that RdRP and components of the RNA interference (RNAi) machinery are necessary to regulate heterochromatin in *S. pombe* and *C. elegans*, it is believed that heterochromatin is regulated in mammals through different mechanisms (7).

Telomerase is a ribonucleoprotein complex that elongates telomeres. Human telomerase reverse transcriptase (hTERT) acts as an RNA-dependent DNA polymerase (RdDP) and synthesizes telomere DNA from a noncoding RNA (ncRNA) template, *hTERC*. Telomere homeostasis mediated by TERT maintains genomic stability and regulates cell life span by maintaining telomeres. However, several lines of evidence suggest that hTERT has functions independent of its known role in telomere maintenance (8–12). Specifically, hTERT expression reduces the number of dicentric chromosomes and suppresses aneuploidy in a manner independent of telomere length (13). In consonance with these observations, hTERT forms several intracellular complexes, only some of which contribute to telomere maintenance (14, 15). For example, hTERT forms a complex with Brahma-related gene 1 (BRG1, or SMARC4) that modulates the transcription of Wnt-dependent genes, such as Myc and cyclin D1 (11). hTERT also interacts with the RNA component of mitochondrial RNA processing endoribonuclease (*RMRP*) to exert RdRP activity, which produces double-stranded RNAs (dsRNAs) that are processed into siRNAs by the RNase III-like enzyme Dicer (10). In addition, we showed that the hTERT/BRG1 complex includes the nucleolar GTP-binding protein, nucleostemin (NS) (this complex will be referred to as TBN), which is essential for maintaining the function of tumor initiating cells (TICs) through telomere-independent mechanisms (15). Together, these studies suggest that hTERT forms multiple complexes with distinct functions in chromosome stability and the maintenance of heterochromatin. Here, we investigated whether hTERT regulates the assembly of heterochromatin in mammalian cells, specifically in complex with BRG1 and NS.

Received 16 January 2014 Returned for modification 30 January 2014
Accepted 10 February 2014
Published ahead of print 18 February 2014
Address correspondence to Kenkichi Masutomi, kmasutom@ncc.go.jp.
Supplemental material for this article may be found at http://dx.doi.org/10.1128/MCB.00093-14.

doi:10.1128/MCB.00093-14

MATERIALS AND METHODS

Generation of an anti-hTERT MAb. Sense and antisense oligonucleotides corresponding to 304 amino acids (aa) to 460 aa of hTERT were purchased from Integrated DNA Technologies Co., Ltd. (IDT) and cloned into plasmid pET-30a(+) (Novagen). A recombinant, carboxyl-terminal His-tagged hTERT protein of 157 amino acids of *hTERT* (position 304 to 460) was overexpressed in *Escherichia coli* and purified by passage through a nickel-agarose column. The recombinant purified hTERT was used as an immunogen to stimulate the production of anti-hTERT monoclonal antibody (MAb) in mice using standard methodologies (16). A sequential screening strategy was used to identify hybridomas producing anti-hTERT MAb. In the initial screen, an enzyme-linked immunosorbent assay (ELISA) was employed to detect hybridomas that produced MAb that bound plate-bound purified His-hTERT. The reactive supernatants were then used in validation experiments described in the legend of Fig. 1.

Absorption of anti-hTERT MAb. An anti-hTERT MAb was first incubated with no peptide or a 1-fold, 10-fold, or 100-fold molar excess of peptide 4 (see Fig. S1 in the supplemental material). After 1 h of incubation at 4°C, the MAb was used for immunofluorescence (IF) or immunoprecipitation (IP) experiments.

Peptide array. Seventy-five peptides derived from a truncated version of hTERT (aa 304 to 460) covalently bound to a continuous cellulose membrane. The panel of peptides was then probed with the anti-hTERT MAb, and bound antibody was detected using Pep Spot (Funakoshi) according to the manufacturer's protocol.

Cell culture and stable expression of hTERT and GFP-hTERT. The human cell lines 293T, HeLa, MCF7, and VA13 and mouse embryonic fibroblasts (MEFs) were maintained in Dulbecco's modified Eagle's medium (DMEM) supplemented with 10% heat-inactivated fetal bovine serum (IFS). The animal experiment protocols were approved by the Committee for Ethics in Animal Experimentation, and the experiments were conducted in accordance with the Guideline for Animal Experiments of the National Cancer Center. HeLa cells and VA13 cells transiently transfected with pNKFLAG-Z-hTERT (10) were used for sucrose density gradient centrifugation and immunoblotting (IB). Amphotropic retroviruses were created as previously described (17) using the vector pBH-hTERT or pMIG-hTERT-GFP (where GFP is green fluorescent protein) (a generous gift from Akira Orimo). Plasmids were transfected using Fugene HD (Roche Diagnostics). After infection, VA13-hTERT cells were selected with hygromycin (100 μg/ml) for 7 days.

Mitotic cell synchronization. The mitotic cell synchronization protocol described by Summers et al. (18) was used. Briefly, cells were switched to medium containing 2.5 mM thymidine (Nacalai Tesque) and incubated for 24 h. Six hours after release, the cells were incubated in medium containing 0.1 μg/ml nocodazole (Invitrogen) for 14 h. After gentle shaking of the dishes, mitotic cells were retrieved.

RT-PCR and quantitative RT-PCR (qRT-PCR). Total cellular RNA was isolated using TRIzol (Invitrogen), treated with DNase (Promega), and subjected to reverse transcription-PCR (RT-PCR). The RT reaction was performed for 60 min at 42°C, followed immediately by PCR (94°C for 30 s, 60°C for 30 s, and 72°C for 30 s). Cycle numbers for PCR are shown in Table S1 in the supplemental material. The *alphoid* reverse primer was labeled with [γ-^{32}P]ATP. *satellite I* primers were used instead of *alphoid* primers to obtain unequivocal PCR products for VA13 cells. Primers used for RT-PCR are listed in Table S1.

Quantitative RT-PCR was performed with a LightCycler 480II (Roche) using LightCycler 480 SYBR green I Master (Roche) according to the manufacture's protocols. Quantitative RT-PCR of Satellite 2 (Sat2) and glyceraldehyde-3-phosphate dehydrogenase (GAPDH) was performed using an Epitect ChIP Antibody Kit for human histone H3 trimethylated at lysine 9 (H3K9me3) (Qiagen) according to the manufacturer's protocols. Human GAPDH, human β-actin, and mouse β-actin genes were used as reference genes. Primers used for qRT-PCR are listed in Table S2 in the supplemental material.

Stable expression of shRNA. We used the pLKO.1-puro vector and the sequences listed in Table S3 in the supplemental material to create short hairpin RNA (shRNA) vectors specific for *hTERT*, *BRG1* (15), *NS* (15), *GFP*, *AGO2*, and *DICER1* (10). These vectors were used to make amphotropic lentiviruses, and polyclonal cell populations were purified by selection with puromycin (2 μg/ml for 3 days).

Antibodies. The following antibodies were used for immunoblotting: anti-FLAG M2 (A2220; Sigma-Aldrich), anti-β-actin AC-15 (A5441; Sigma-Aldrich), anti-NS (A300-600A; Bethyl Laboratories), anti-BRG1 (a gift from Tsutomu Ohta, National Cancer Center), anti-phospho-histone H3 (Ser10) (pHH3^{Ser10}, (06-570; Millipore), anti-H3K9me3 (07-442; Millipore), anti-histone H3 (06-755; Millipore), anti-DICER 13D6 (ab14601; Abcam), anti-AGO2 4G8 (015-22031; Wako), and anti-hTERT MAb (clone 10E9-2).

The following antibodies were used for immunoprecipitation (IP), IP–RT-PCR, IP-telomere repeat amplification protocol (TRAP), and chromatin immunoprecipitation (ChIP): anti-hTERT MAb (clone 10E9-2), anti-AGO2 4G8 (015-22031; Wako), anti-H3K9me3 (ab8898; Abcam), ChromPure mouse IgG (015-000-003; Jackson ImmunoResearch), and ChromPure rabbit IgG (011-000-003; Jackson ImmunoResearch).

The mouse MAbs used for immunofluorescence analysis were anti-hTERT MAb (clone 10E9-2), anticoilin IH10 (ab87913; Abcam), anti-centromere protein A (CENPA) 3-19 (D115-3; Medical and Biological Laboratories Co., Ltd.), and anti-AGO2 4G8 (015-22031; Wako). The rabbit MAb used was anti-CENPA EP800Y (04-205; Millipore). The rabbit polyclonal antibodies used were anti-NS (A300-600A; Bethyl laboratories), anti-BRG1 (a gift from Tsutomu Ohta, National Cancer Center), anti-pHH3^{Ser10} (06-570; Millipore), anti-α-tubulin DM1A (T6199; Sigma-Aldrich), anti-H3K9me3 (07-442; Millipore), and anti-HP1β (07-333; Millipore). The rat MAb used was anti-α-tubulin YL1/2 (ab6160; Abcam). The goat polyclonal antibody used was anti-TRF2 (IMG-148A; Imgenex). The following secondary antibodies were used: Alexa Fluor 488-, 568-, or 647-conjugated goat anti-mouse, -rabbit, or -rat IgG (Invitrogen) and Alexa Fluor 488- or 568-conjugated donkey anti-mouse or -goat IgG (Invitrogen).

Immunoblotting. Cells were lysed in radioimmunoprecipitation assay (RIPA) buffer containing 1% NP-40, 1 mM EDTA, 50 mM Tris-HCl (pH 7.4), and 150 mM NaCl. After sonication, lysates were cleared of insoluble material by centrifugation at 21,000 × *g* at 4°C for 15 min. Proteins (100 μg) were subjected to SDS-PAGE in 6%, 8%, or 12% polyacrylamide gels, followed by immunoblot analysis.

Immunoprecipitation. For IP followed by immunoblotting, cells were lysed in lysis buffer A (LBA) containing 0.5% NP-40, 20 mM Tris-HCl (pH 7.4), and 150 mM NaCl. After sonication, lysates were cleared of insoluble material by centrifugation at 21,000 × *g* at 4°C for 15 min, followed by the addition of 20 μl of prewashed 1:1 slurry of anti-FLAG M2 Affinity gel (Sigma-Aldrich) or 4 μg of antibody and 30 μl of Pierce protein A plus agarose (Thermo Scientific) and incubation overnight at 4°C. The bead complexes were washed three times with LBA and eluted in 2× SDS loading buffer containing 20% β-mercaptoethanol, 20% glycerol, 4% SDS, and 100 mM Tris-HCl (pH 7.4), followed by SDS-PAGE and immunoblot analysis.

For IP followed by RT-PCR, cells were lysed in LBA. After a 30-min incubation on ice, lysates were cleared of insoluble material by centrifugation at 21,000 × *g* at 4°C for 15 min. The whole-cell lysates were incubated overnight with 4 μg of antibody and 30 μl of Pierce protein A plus agarose at 4°C. The protein A bead complexes were then washed three times with LBA, eluted in TRIzol, and analyzed by RT-PCR.

Sucrose density gradient centrifugation. HeLa cells overexpressing FLAG-hTERT were lysed in LBA and incubated on ice for 30 min. Lysates were cleared of insoluble material by centrifugation at 21,000 × *g* at 4°C for 30 min. Five hundred microliters of lysate (5 μg/μl protein concentration) was loaded onto 5 ml of a preformed 15 to 37.5% sucrose-LBA gradient and centrifuged for 17 h at 130,000 × *g* using a P40ST rotor in an ultracentrifuge (Hitachi). After centrifugation, the contents were ali-

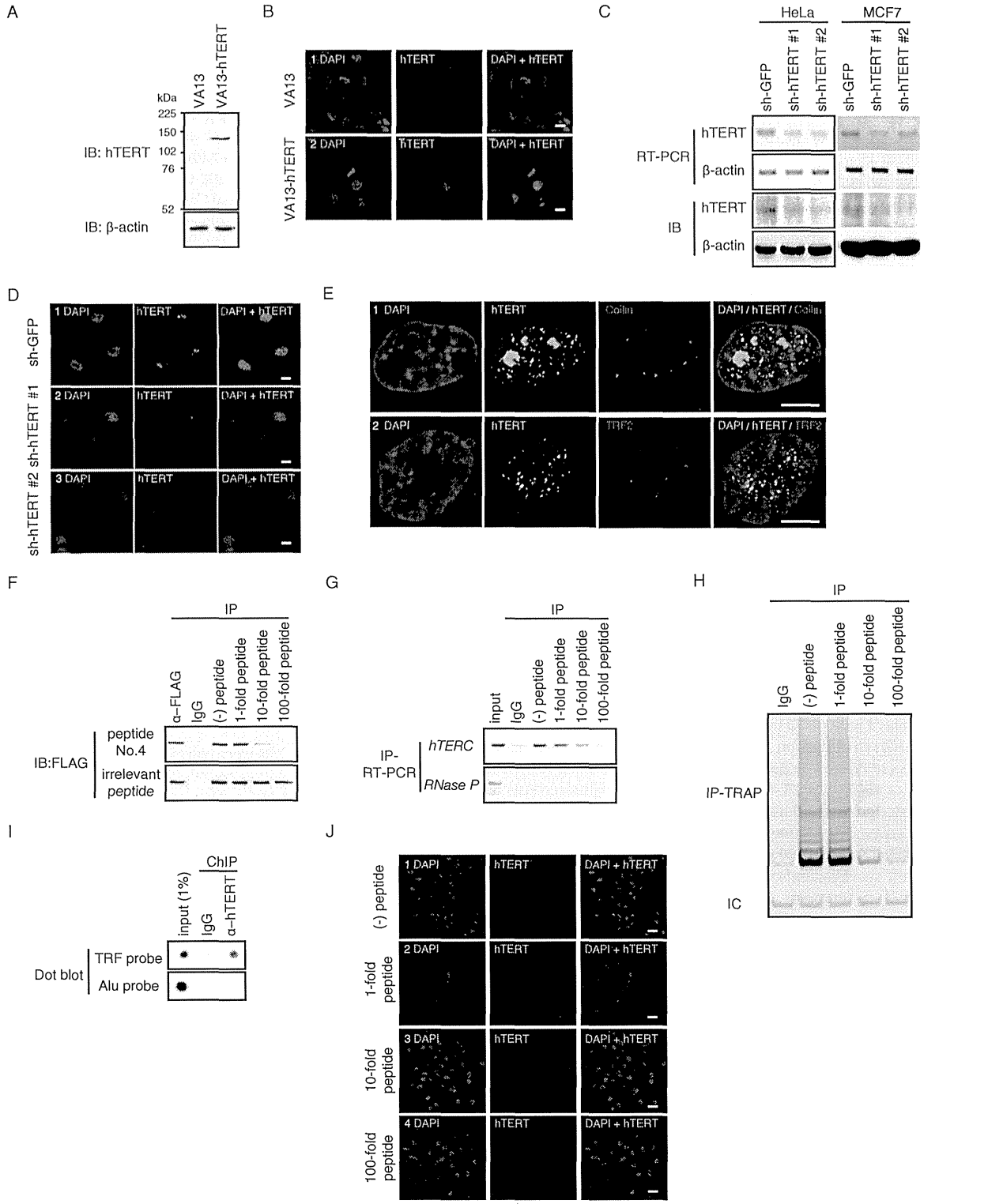

FIG 1 Validation of the anti-hTERT MAb. (A) Immunoblot (IB) of ectopically expressed hTERT using an anti-hTERT MAb. hTERT was transiently expressed in VA13 cells and immunoblotted with the 10E9-2 anti-hTERT MAb. (B) Immunofluorescence (IF) of hTERT and DAPI in VA13 cells. VA13 and VA13-hTERT cells were immunostained with the 10E9-2 MAb followed by DAPI staining. Scale bar, 10 μm. (C) RT-PCR or IB of hTERT expression in HeLa or MCF7 cells expressing control (shRNA to *GFP*) or *hTERT*-specific shRNAs. β-Actin, internal control. (D) IF of hTERT in HeLa cells expressing sh-*GFP* as a control, sh-*hTERT* 1, or sh-*hTERT* 2. Representative images are shown. Scale bar, 10 μm. (E) Colocalization of hTERT with coilin or TRF2. HeLa cells were immunostained with anti-hTERT MAb and anticoilin antibodies (row 1) or anti-TRF2 antibodies (row 2) followed by DAPI staining. Scale bar, 10 μm. (F) Immunoprecipitation (IP) of overexpressed hTERT using anti-hTERT MAb. FLAG-tagged hTERT was transiently expressed in 293T cells, and immune complexes were isolated using anti-hTERT MAb incubated with or without peptide 4 or irrelevant peptide (peptide 5) and immunoblotted with the FLAG-M2 antibody. (G) IP of endogenous hTERT using anti-hTERT MAb. Immune complexes were isolated from HeLa cells using anti-hTERT MAb incubated

quoted into 10 consecutive fractions (F1 to F10) with a volume of 500 μl each, and the fractions were sequentially numbered from high density (F1) to low density (F10). Seventy-five microliters of each fraction was used for immunoblotting.

TRAP assay. A telomeric repeat amplification protocol (TRAP) was used to detect telomere-specific reverse transcriptase activity as described previously (19).

Immunofluorescence. HeLa, VA13, or MCF7 cells (2.8×10^4 cells) were seeded onto eight-well culture slides (BD). The cells were fixed using a protocol based on that described by Thibault and Buschmann (20). Briefly, 1 day after seeding, cells were washed twice with phosphate-buffered saline not containing either calcium ions or magnesium ions [PBS(−)] and fixed in PBS(−) containing 1% paraformaldehyde and 0.5% Triton X-100 at 37°C for 20 min. Then, the cells were washed three times in PBS(−), followed by a 30-min incubation in PBS(−) containing 100 mM glycine at room temperature. All immunocytochemical reactions were performed at room temperature, unless otherwise specified. The fixed cells were incubated for 2 h or at 4°C overnight with PBS(−) containing 5% bovine serum albumin Cohn fraction V (WAKO) to block nonspecific reactions. The fixed cells were incubated first with primary antibody at room temperature for 2 h or at 4°C overnight. After cells were washed four times with PBS(−), they were incubated with secondary antibodies for 1.5 h. After another four washes in PBS(−), the cells were mounted in Vectashield containing 4′,6′-diamidino-2-phenylindole (DAPI; Vector Laboratories) and imaged under a laser scanning microscope (TCS SP2; Leica Microsystems). To analyze the mitotic index in the cells expressing shRNAs, HeLa cells were infected with lentiviruses to express shRNAs, and polyclonal cell populations were purified by selection with puromycin. Four days after infection, the cells were fixed. For analyzing DNA fluorescence intensity, the cells were treated with PBS(−) containing 1 mM Hoechst 33342 (Invitrogen) for 20 min at room temperature, followed by two washes in PBS(−). The cells were then observed under a spinning-disk confocal microscope (IX-81 with DSU; Olympus Corporation).

DNA content analysis. DNA content analysis was performed with a JSAN cell sorter (Bay Bioscience) using a Cycletest Plus DNA reagent kit (BD Bioscience) according to the manufacturer's protocols.

IP-RdRP assay. IP followed by an RdRP (IP-RdRP) assay was modified from the original protocol (21). For the assay, 1×10^7 cells were lysed in 1 ml of lysis buffer A (0.5% NP-40, 20 mM Tris-HCl [pH 7.4], and 150 mM NaCl). After sonication, lysates were cleared of insoluble material by centrifugation at 21,000 × *g* at 4°C for 15 min. The lysate was preabsorbed with 40 μl of Pierce protein A plus agarose (Thermo Scientific) for 30 min. Preabsorbed lysate was mixed with 10 μg of anti-hTERT MAb (clone 10E9-2), anti-BRG1 antibody (ab4081; Abcam), or anti-NS antibody (A300-599A; Bethyl Laboratories) and 40 μl of Pierce protein A plus agarose and incubated overnight at 4°C. Immune complexes were washed four times with 1× acetate buffer (10 mM HEPES-KOH [pH 7.8], 100 mM potassium acetate, and 4 mM $MgCl_2$) containing 10% glycerol, 0.1% Triton X, and 0.06× protease inhibitor and once with AGC solution [1× acetate buffer, 10% glycerol, and 0.02% 3-[(3-cholamidopropyl)-dimethylammonio]-1-propanesulfonate (CHAPS) containing 2 mM $CaCl_2$. The bead suspension was treated with 0.25 unit/μl MNase at 25°C for 15 min. The immunoprecipitates were subsequently washed twice with AGC solution containing 3 mM EGTA and once with 1× acetate buffer containing 0.02% CHAPS. Finally, 40 μl of a reaction mixture was prepared from 20 μl of the bead suspension, 6 μl of [α-^{32}P]UTP (3,000 Ci/mmol), a final 25 ng/μl of RNA template, and supplements and incubated at 32°C for 2 h. The final concentrations of ribonucleotides were 1 mM ATP, 0.2 mM GTP, 10.5 μM UTP, and 0.2 mM CTP. The resulting products were treated with proteinase K to stop the reaction, purified several times with phenol-chloroform until the white interphase was gone, and precipitated using ethanol. For a UTP incorporation assay, RdRP products were treated with RNase I (2 U; Promega) at 37°C for 2 h to digest single-stranded RNAs (ssRNAs) and RNase V1 (0.2 U; Ambion) at 37°C for 1 h to digest dsRNAs, followed by proteinase K treatment, phenol-chloroform purification, and ethanol precipitation. In the Northern blotting experiment that examined antisense RNA synthesized by hTERT, nonlabeled UTP was used instead of [α-^{32}P]UTP. Synthetic RNAs used as templates for IP-RdRP assays were the following: synthetic RNA 1, 5′-GGGUUUAAAAUGUAAUAGGACCCACAUGAUCCCA-3′; synthetic RNA 2, 5′-GGGAUCAUGUGGGUCCUAUUACAUUUUAAACCCA-3′.

Northern blotting. Small RNAs (<200 nucleotides in length) were isolated using a mirVana miRNA Isolation Kit (Ambion) according to the manufacturer's protocol. Ten micrograms of small RNA or the product of the IP-RdRP assay was separated on denaturing 20% or 10% polyacrylamide gels and then blotted onto Hybond-N^+ membranes (GE Healthcare) using a Trans-Blot SD semidry transfer cell (Bio-Rad). Hybridization was performed in Church buffer (0.5 M $NaHPO_4$ [pH 7.2], 1 mM EDTA, and 7% SDS) containing 1×10^6 cpm/ml of ^{32}P-labeled sense probe derived from nucleotides 229 to 267 of *RMRP*, antisense probe derived from nucleotides 1 to 70 of *hLINE1*, or antisense probe derived from nucleotides 120 to 171 of *alphoid* for 14 h. The membranes were washed in 2× SSC (1× SSC is 0.15 M NaCl plus 0.015 M sodium citrate), and the signals were detected by autoradiography.

Chromatin immunoprecipitation (ChIP). HeLa cells (1×10^7 cells) were cross-linked with 1% paraformaldehyde (Nacalai Tesque) in culture medium for 10 min at room temperature. After aldehydes were quenched with PBS(−) containing 200 mM glycine (Sigma-Aldrich) for 5 min followed by a PBS(−) wash, the fixed cells were harvested with 1 ml of NP-40 buffer (10 mM Tris-HCl [pH 8.0], 10 mM NaCl, and 0.5% NP-40) using a cell scraper (Costar) and centrifuged at 1,000 × *g* at 4°C for 3 min. The cell pellets were resuspended in 100 μl of SDS lysis buffer B (50 mM Tris-HCl [pH 8.0], 1% SDS, and 10 mM EDTA) and 400 μl of ChIP dilution buffer (50 mM Tris-HCl [pH 8.0], 167 mM NaCl, 1.1% Triton X-100, and 0.11% sodium deoxycholate) containing 1% protease inhibitor cocktail [4-(2-aminoethyl) benzenesulfonyl fluoride hydrochloride (AEBSF), aprotinin, E-64, leupeptin hemisulfate monohydrate; Nacalai Tesque]. The lysate was sonicated using a sonication system (Bioruptor, CosmoBio). The sonicated lysate was centrifuged at 20,000 × *g* at 4°C for 10 min, and the supernatant was transferred to new tubes. ChIP dilution buffer (500 μl) was added to the supernatant, and 100 μl of the supernatant was set aside for input. One hundred microliters of 1× RIPA buffer A (50 mM Tris-HCl [pH 8.0], 150 mM NaCl, 1 mM EDTA, 0.1% SDS, 1% Triton X-100, and 0.1% sodium deoxycholate) was added to the supernatant. The supernatant was precleared using protein G-Sepharose beads (GE Healthcare) at 4°C for 2 h, followed by centrifugation at 9,000 × *g* at 4°C for 1 min. The supernatant was then transferred to new tubes. Antibodies were added to the supernatant, and the tubes were rotated overnight at 4°C. Protein G-Sepharose beads blocked by DMEM supplemented with 10% IFS were then added, and the samples were rotated for another 2 h at 4°C. The antibody-protein G-Sepharose complex was washed with 1× RIPA buffer A at 4°C for 5 min followed by a wash with 1× RIPA buffer B (50 mM Tris-HCl [pH 8.0], 500 mM NaCl, 1 mM EDTA, 0.1% SDS, 1% Triton X-100, and 0.1% sodium deoxycholate) and two washes with TE buffer (10 mM Tris-HCl [pH 8.0] and 1 mM EDTA) at 4°C for 5 min. ChIP elution buffer (200 μl; 10 mM Tris-HCl [pH 8.0], 300 mM NaCl, 5 mM EDTA, and 0.5% SDS) was added and incubated at

with or without antigen peptides, and *hTERC* and RNase P RNA were detected by RT-PCR. (H) IP-TRAP of endogenous hTERT from HeLa cells. IC, internal control. (I) ChIP performed in HeLa cells using the anti-hTERT MAb. Dot blot signals were detected with the indicated γ-^{32}P-labeled probes. (J) IF of hTERT and DAPI in HeLa cells. Cells were immunostained with anti-hTERT MAb incubated with no peptide [(−) peptide] or a 1-, 10-, or 100-fold molar excess of peptide 4. Representative images are shown. Scale bar, 10 μm.

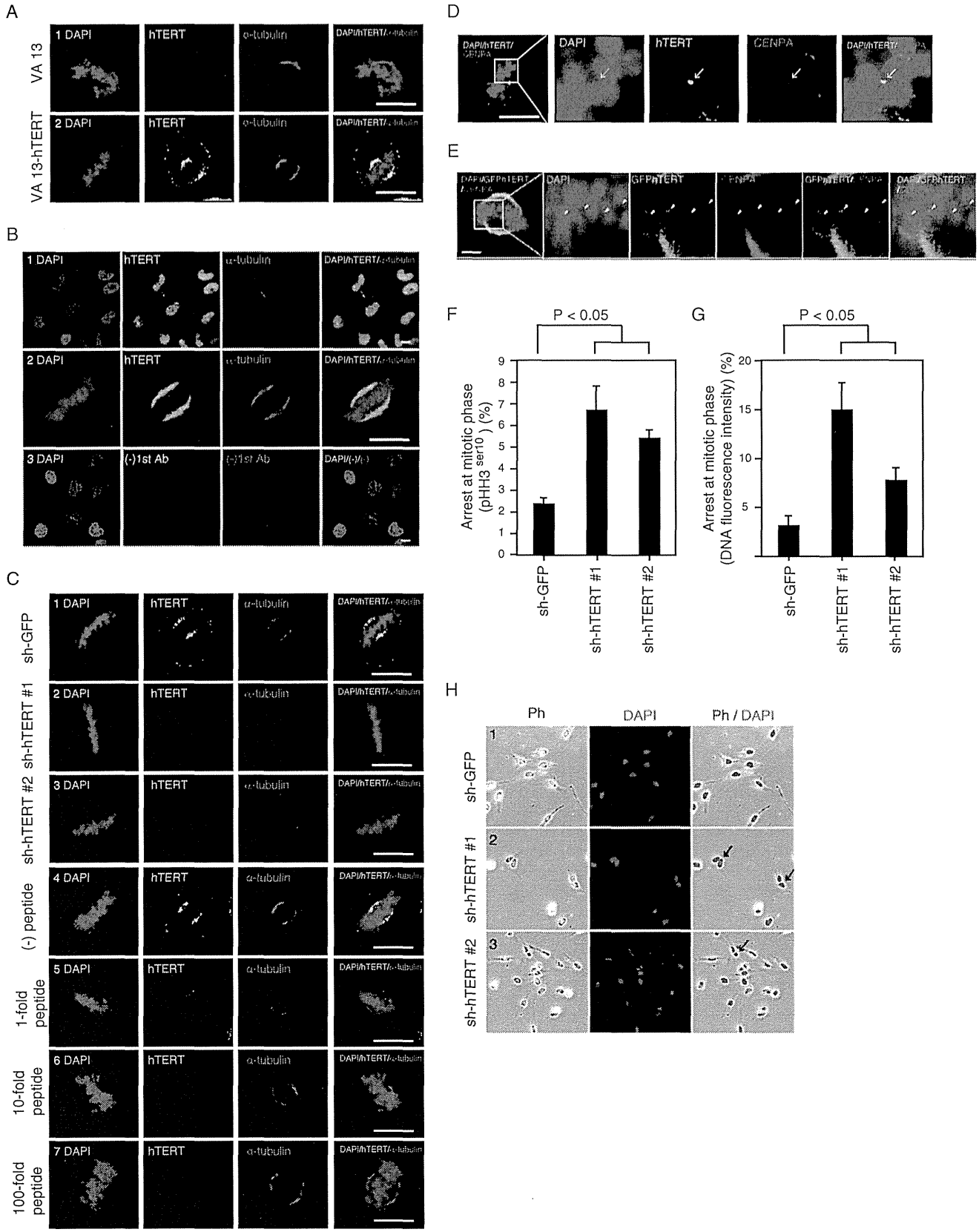

FIG 2 hTERT localizes to both mitotic spindles and centromeres. (A) Immunofluorescence (IF) of hTERT, α-tubulin, and DAPI in VA13 cells. VA13 and VA13-hTERT cells were immunostained with the 10E9-2 anti-hTERT MAb and anti-α-tubulin antibodies followed by DAPI staining. Scale bar, 10 μm. (B) IF of hTERT, α-tubulin, and DAPI in HeLa cells in interphase (rows 1 and 3) or in mitosis (row 2). HeLa cells were not immunostained [(−)1st

65°C overnight. After the incubation, 4 μg of RNase A (Invitrogen) was added and incubated at 37°C for 30 min. Proteinase K (20 μg) was then added, and the sample was incubated at 55°C for 1 h. DNA was then purified using a standard phenol-chloroform extraction followed by ethanol precipitation and was resuspended in TE buffer.

Dot blot analysis. DNA retrieved by ChIP was denatured at 100°C for 10 min in 400 mM NaOH and 10 mM EDTA. Denatured samples were dotted onto a Hybond-XL membrane (Amersham) using a Bio-Dot Apparatus (Bio-Rad). The membrane was baked at 80°C and prehybridized with Church buffer (0.5 M $NaHPO_4$ [pH 7.2], 1 mM EDTA, 3% SDS) at 37°C for 2 h. After prehybridization, γ-^{32}P-labeled probes were added and hybridized at 37°C overnight. After hybridization, the membrane was rinsed twice with 10 ml of 2× SSC containing 0.1% SDS followed by two washes with 50 ml of 2× SSC containing 0.1% SDS for 10 min, two washes with 50 ml of 1× SSC containing 0.1% SDS for 10 min, and four washes with 50 ml of 0.1× SSC containing 0.1% SDS for 5 min. The washing steps were done at 37°C. Probes labeled with [γ-^{32}P]ATP using T4 polynucleotide kinase (TaKaRa Bio, Inc.) were the following: *TRF* probe, (5′-CCC TAACCCTAACCCTAA-3′; *Alu* probe, 5′-CGGAGTCTCGCTCTGTCG CCCAGGCTGGAGTGCAGTGGCGCGA-3′; *alphoid* probe, 5′-AGTTT CTGAGAATCATTCTGTCTAG-3′; *hLINE1* probe, 5′-CGGAAGAGTG TCTGGAGCAA-3′.

AZA, 5-aza-dC, and TSA treatment. For treatment of 5-azacytidine (AZA) and trichostatin A (TSA), HeLa cells were switched to medium containing 10 μM AZA (Sigma-Aldrich) for 24 h followed by treatment with 0.5 μM TSA (Sigma-Aldrich) for 12 h. For treatment of 5-aza-deoxycytidine (5-aza-dC) and TSA, HeLa cells were switched to medium containing 0.3 μM 5-aza-dC (Sigma-Aldrich) twice for 48 h and 24 h followed by treatment of 0.5 μM TSA for 24 h.

RESULTS

hTERT localizes to both mitotic spindles and centromeres. TERT protein is expressed at low levels even in human cancer cell lines (22). To facilitate the study of hTERT, we generated a new anti-hTERT monoclonal antibody (MAb) (clone 10E9-2) by immunizing mice with a recombinant truncated version of hTERT (amino acids 304 to 460). Using this MAb, we detected ectopically expressed hTERT in VA13 cells, known to lack hTERT, by immunoblotting (IB) (Fig. 1A) and immunofluorescence (IF) (Fig. 1B). We also demonstrated that the 10E9-2 MAb detected endogenous TERT in the HeLa and MCF7 human cancer cell lines (Fig. 1C and D). Expression of two different *hTERT*-specific short hairpin RNAs (shRNAs) in these cells suppressed *hTERT* mRNA expression and endogenous protein expression in both cell lines (Fig. 1C and D). We found that hTERT colocalized with coilin, a marker for Cajal bodies (14), or TRF2, a component of shelterin complex which locates at telomeres during S phase (23, 24), in HeLa cells (Fig. 1E). Because we used asynchronously dividing cells, not all of TRF2 colocalized with hTERT as reported previously (25). To confirm the specificity of 10E9-2, we mapped the epitope recognized by this MAb by testing reactivity to 75 peptides spanning amino acids 304 to 460 of hTERT (see Fig. S1A in the supplemental material) and found that peptide 4 (sequence, TSRPPRPWDT) was recognized by this MAb (see Fig. S1B). We then showed that the addition of peptide 4 but not an irrelevant peptide (peptide 5) (see Fig. S1B) inhibited the ability to isolate exogenous (Fig. 1F) or endogenous hTERT immune complexes (Fig. 1F to H) as assessed by IB, measuring *hTERC* levels, or TRAP assay. Furthermore, we performed a ChIP assay using this MAb and detected a strong signal by a telomere restriction fragment (TRF) probe (Fig. 1I) (26). When we performed IF, peptide 4 inhibited the signal from this antibody binding to endogenous hTERT (Fig. 1J). Taken together, these observations confirm that the 10E9-2 MAb recognizes endogenous hTERT.

To determine the subcellular localization of hTERT, we performed IF experiments in VA13, VA13-hTERT, and human cancer cell lines. Although we failed to detect hTERT in VA13 cells in any phase of the cell cycle (Fig. 1B and 2A), we found that hTERT localized to mitotic spindles, as assessed by colocalization with α-tubulin, in VA13-hTERT cells (Fig. 2A) and HeLa cells (Fig. 2B). The expression of *hTERT*-specific shRNAs (Fig. 2C, upper panels) or introduction of peptide 4 (Fig. 2C, lower panels) eliminated this staining pattern. We also confirmed that hTERT colocalized with CENPA, a centromeric marker (Fig. 2D and E), during mitosis, which indicates that hTERT localized not only on mitotic spindles but also at centromeres. Although hTERT associates with telomeres during S phase (26), TRF1 and TRF2 create a closed configuration of telomeres during mitosis that prevents telomerase from elongating telomeres (27). Based on these observations, we concluded that TERT is localized to mitotic spindles and centromeres in mitosis.

To determine whether the association of hTERT with mitotic spindles and centromeres exerts an influence on their function, we assessed mitotic progression in cells expressing control or *hTERT*-specific shRNAs by measuring phospho-histone H3^{Ser10} (pHH3^{Ser10}) (Fig. 2F) or DNA fluorescence intensity (Fig. 2G). We found that the percentage of cells arrested in mitosis was increased 2- to 5-fold in cells in which hTERT was suppressed compared to cells expressing shRNA targeting *GFP* (sh-*GFP*) (*P* values of <0.05) (Fig. 2F and G). At the same time, we found an increased ratio of binucleate cells in HeLa cells expressing sh-*hTERT* (sh-*hTERT* 1, 3.6%, or 16/443 cells; sh-*hTERT* 2, 2.6%, or 9/350 cells) compared to those expressing sh-*GFP* (0.34%, 2/591 cells) (Fig. 2H). We confirmed that under these conditions, expression of these shRNAs did not alter cell viability (10). These observations demonstrate that the suppression of hTERT inhibits mitotic progression.

hTERT regulates gene expression from centromeres and retrotransposons and is essential for heterochromatin assembly. The maintenance of heterochromatin at centromeres and other

Ab] or were immunostained with anti-hTERT MAb and anti-α-tubulin antibodies followed by DAPI staining. Scale bar, 10 μm. (C) IF of hTERT, α-tubulin, and DAPI in HeLa cells. Suppression of hTERT (sh-*GFP* as a control) was observed by immunofluorescence. MAb was incubated with no peptide [(−) peptide] and a 1-, 10-, or 100-fold molar excess of antigen peptide. HeLa cells were immunostained with anti-hTERT MAb and anti-α-tubulin antibodies followed by DAPI staining. Representative images are shown. Scale bar, 10 μm. (D) Colocalization of hTERT and CENPA. HeLa cells were immunostained with anti-hTERT MAb and anti-CENPA antibodies followed by DAPI staining. The image in the rectangle shown in the left panel is magnified and shown on the right. Arrow denote colocalization of hTERT with CENPA. Scale bar, 10 μm. (E) Colocalization of GFP-hTERT and CENPA. HeLa-GFP-hTERT cells were immunostained with anti-CENPA followed by DAPI staining. The image in the rectangle shown in the left panels is magnified and shown on the right. Arrowheads denote colocalization of GFP-hTERT with CENPA. Scale bar, 5 μm. (F) A graph of the mitotic arrest according to pHH3^{Ser10} immunofluorescence in HeLa cells expressing shRNAs. The *P* value for sh-*hTERT* versus sh-*GFP* was <0.05. (G) A graph of the mitotic arrest according to DNA fluorescence intensity and the morphology of HeLa cells expressing shRNAs. The *P* value for sh-*hTERT* versus sh-*GFP* was <0.05. (H) Binucleate formation of HeLa cells with sh-*hTERT*. HeLa cells expressing sh-*GFP*, sh-*hTERT* 1, or sh-*hTERT* 2 were stained with DAPI. Arrow denote binucleate cells. Ph, phase-contrast image.

regions is essential for proper chromosomal segregation during mitosis in *S. pombe* (28), *C. elegans* (5, 6), and human cells (29). Using nocodazole treatment to arrest cells in mitosis as assessed by staining for $pHH3^{Ser10}$ (Fig. 3D) and examining the cell cycle distribution of treated cells (Fig. 3A), we monitored the expression of transcripts from centromeric alpha-satellite (*alphoid*) repeat elements (30) and the noncentromeric long interspersed repeat element 1 (*LINE1*) (31) in HeLa cells or VA13 cells. We confirmed that the expression of *alphoid* and *hLINE1* transcripts was tightly suppressed during mitosis in HeLa cells (Fig. 3B). In consonance with these findings, we found baseline levels of histone H3 trimethylated at Lys9 (H3K9me3), a marker for silent chromatin (32), at telomeres and *alphoid* and *hLINE1* elements in cycling cells (Fig. 3C) and increased levels of H3K9me3 in HeLa cells treated with nocodazole (Fig. 3D). To confirm that the expression of *alphoid* or *hLINE1* RNA levels represented the heterochromatic state of these regions, we exposed these cells to trichostatin A (TSA) and two inhibitors of DNA methyltransferase, 5-azacytidine (AZA) and 5-aza-deoxycytidine (5-aza-dC) (33), and found that cells treated with these agents overexpressed *alphoid* or *hLINE1* RNA and showed downregulation of H3K9me3 marks at *alphoid* and *hLINE1* regions (Fig. 3E and F). These observations confirmed that *alphoid* and *hLINE1* are regulated by the state of heterochromatin.

To assess the consequences of suppressing hTERT on the expression and chromatin state of these regions, we monitored the expression level of *alphoid* and *hLINE1* in cells which we suppressed hTERT. Specifically, we monitored the *alphoid* and *hLINE1* RNA expression levels in HeLa and MCF7 cells in which endogenous hTERT was depleted by two independent shRNAs (Fig. 1C and D). Suppressing hTERT resulted in increased transcription of both sense and antisense RNAs from *alphoid* and *hLINE1* elements as assessed by quantitative RT-PCR in HeLa (Fig. 4A) or MCF7 cells (Fig. 4B). Moreover, when we suppressed TERT expression by *TERT*-specific shRNAs, we found decreased expression of the H3K9me3 and HP1-β marks, which associate with heterochromatic regions (Fig. 4C and D). These experiments show that suppression of TERT leads to alterations in chromatin.

Telomeres in most inbred murine strains are longer than human telomeres, and murine TERT (mTERT) is constitutively expressed in many somatic tissues, leading to differences in telomere biology. To examine whether mTERT is also essential for heterochromatin maintenance, we investigated the transcription of transcripts from three murine transposon families: murine intracisternal A particles (*IAP*) (34), murine *LINE1* (*mLINE1*) *Type A* and *mLINE1 Type Tf* (35). Using mouse embryonic fibroblast (MEF) cells derived from $mTERT^{-/-}$ or $mTERT^{+/+}$ mice (Fig. 4E), we found that transcripts from *IAP*, *mLINE1 Type A* and *mLINE1 Type Tf* were upregulated in $mTERT^{-/-}$ MEFs compared with levels in $mTERT^{+/+}$ MEFs (Fig. 4F) (P values of <0.05). $mTERT^{-/-}$ MEF cells, however, did not show increased binucleate formation (4.8%; 22/463 cells) compared to those of $mTERT^{+/+}$ MEF cells (6.7%; 28/415 cells). We believe that the observed difference between HeLa cells with shRNAs and $mTERT^{-/-}$ MEFs is likely due to the difference between acute suppression and germ line deletion of the target gene. In animals that lack *mTERT*, the effects of loss of mTERT may be partially compensated by another factor(s) to maintain chromosome segregation. Taken together, these observations confirm that manipulation of TERT levels affects heterochromatin maintenance in both human and murine cells.

To further confirm the role of TERT in regulating the expression of these genes, we tested whether inhibiting hTERT enzymatic activity with the telomerase inhibitor β-rubromycin (36) affected the expression of transcripts from these regions. We confirmed that β-rubromycin inhibits both telomerase and RdRP activity (Fig. 4G) and found that transcription of *alphoid* and *hLINE1* RNAs was upregulated in cells treated with β-rubromycin in HeLa cells but not in VA13 cells (Fig. 4H). Collectively, these observations suggest that TERT regulates the expression of centromeric repeated elements and transposons in a manner that correlates with the status of heterochromatin at these loci.

Single-stranded RNAs transcribed from *alphoid* or *hLINE1* elements interact with hTERT. TERT binds to telomeric regions through interactions with specific telomere binding proteins. To investigate whether hTERT binds directly to centromeres or *hLINE1*, we performed chromatin immunoprecipitation (ChIP) to determine whether we could detect *alphoid* or *hLINE1* elements in hTERT immune complexes under conditions in which we detected telomere restriction fragments (Fig. 1I) (26). Although we failed to detect *alphoid* or *hLINE1* elements in cycling cells, both *alphoid* and *hLINE1* elements were observed in hTERT immune complexes isolated from cells treated with nocodazole (Fig. 4I), suggesting that hTERT associates with these regions during mitosis.

In *S. pombe*, siRNAs that are complementary to nascent centromeric RNA recruit the RITS complex to centromeric regions to form heterochromatin (1–3) in a manner that requires the *S. pombe* RdRP Rdp1. In prior work, we found that an *hTERC*-independent, hTERT-*RMRP* complex exhibited RdRP activity (10). To determine whether TERT also binds other noncoding RNAs transcribed from *alphoid* or *hLINE* elements, we isolated hTERT immune complexes and probed for RNAs corresponding to these RNAs (Fig. 4J, left panels). To confirm that hTERT interacts with single-stranded RNAs (ssRNAs), we then tested whether treatment of these hTERT-specific immune complexes with RNase I, which specifically digests ssRNAs, affected these RNAs. We found that RNase I treatment abolished the binding of all of these RNA species (Fig. 4J, right panels), suggesting that hTERT interacts with ssRNAs.

Enrichment of RdRP activity of hTERT during mitosis. In *S. pombe* (28) and *C. elegans* (5, 6), the recruitment of RITS to heterochromatic regions requires the synthesis of dsRNAs and processing to siRNAs. To assess hTERT-associated RdRP activity, we established an IP-RdRP assay by modifying a method used to analyze the *C. elegans* RdRP (21). Specifically, we isolated hTERT immune complexes from cells treated with nocodazole (manipulated) or dimethyl sulfoxide (DMSO; unmanipulated) and performed the RdRP assay. We first confirmed that the observed products were dsRNAs by treating the products with RNase I. This protocol also eliminated products produced by hTERT-associated terminal transferase activity (37).

Using HeLa cells arrested in mitosis, we isolated hTERT immune complexes and performed an RdRP assay (IP-RdRP assay) using *RMRP* RNA (10) as a template (Fig. 5). We found 267-nucleotide (nt), RNase I-resistant products corresponding to *RMRP* in nocodazole-treated cells (Fig. 5B). We noted a collection of radioactive short RNA species in IP-RdRP assays using cells treated with nocodazole (Fig. 5B) that may represent intermediate

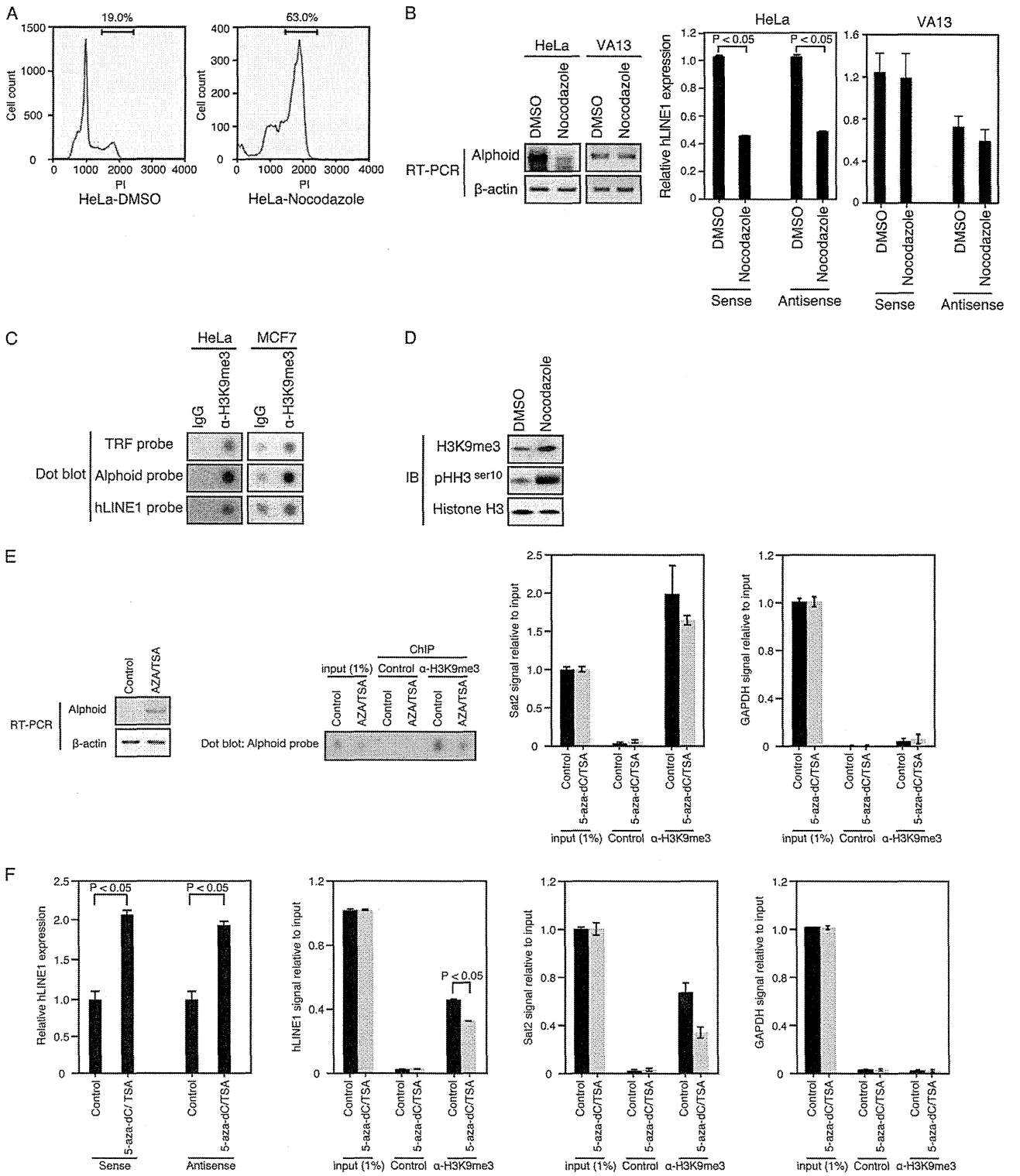

FIG 3 Expression of *alphoid* and *hLINE1* is regulated by the state of heterochromatin. (A) DNA content analysis of cells treated with DMSO or nocodazole. The cell fractions in G_2/M phase were 19% (DMSO) and 63% (nocodazole). (B) RT-PCR of *alphoid* and qRT-PCR of *hLINE1* RNA expression levels in HeLa or VA13 cells treated with nocodazole (manipulated) or DMSO (unmanipulated). The *alphoid* DNA PCR products are 171 bp, or multiples of 171 bp (56). A representative band is shown. β-Actin, internal control. *P* values for nocodazole versus DMSO were <0.05. (C) ChIP performed in HeLa or MCF7 cells using anti-H3K9me3 antibody. Dot blot signals were detected with the indicated γ-^{32}P-labeled probes. (D) Immunoblot (IB) analysis using the indicated antibodies in HeLa cells treated with nocodazole or DMSO. Histone H3, internal control. (E) RT-PCR of *alphoid* and ChIP using anti-H3K9me3 Ab. Dot blot signals were detected with the γ-^{32}P-labeled *alphoid* probes. HeLa cells were treated with AZA (10 μM) followed by TSA (0.5 μM). Satellite 2 (Sat2) (positive control) and *GAPDH* (negative control) were used as controls for ChIP using anti-H3K9me3 Ab. (F) qRT-PCR of *hLINE1* and ChIP using anti-H3K9me3 Ab. HeLa cells were treated with 5-aza-dC (0.3 μM) followed by TSA (0.5 μM). α, anti.

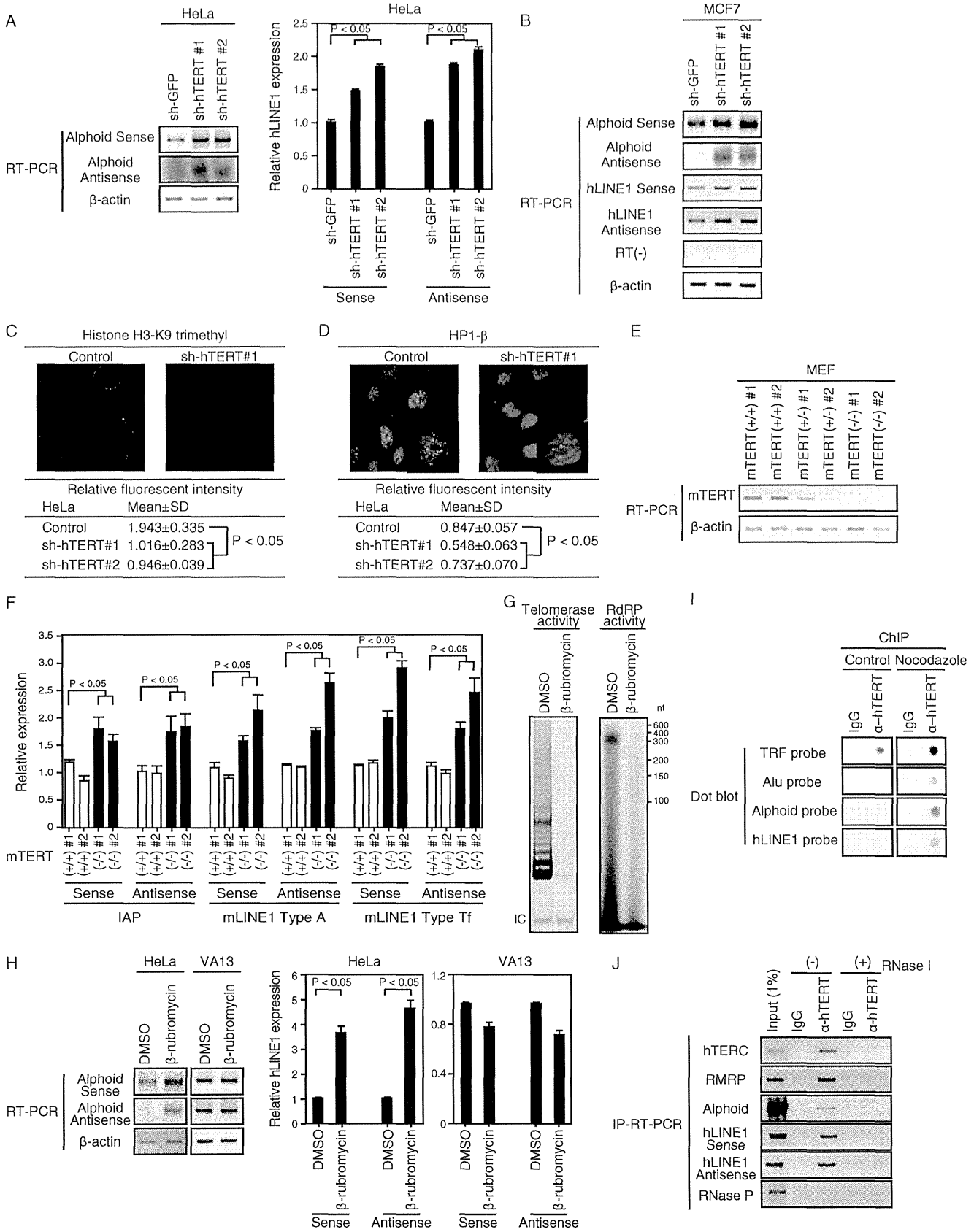
A
HeLa
sh-GFP
sh-hTERT #1
sh-hTERT #2
RT-PCR
Alphoid Sense
Alphoid Antisense
β-actin
HeLa
Relative hLINE1 expression
P < 0.05
P < 0.05
Sense
Antisense
B
MCF7
sh-GFP
sh-hTERT #1
sh-hTERT #2
RT-PCR
Alphoid Sense
Alphoid Antisense
hLINE1 Sense
hLINE1 Antisense
RT(-)
β-actin
C
Histone H3-K9 trimethyl
Control
sh-hTERT#1
Relative fluorescent intensity
HeLa Mean±SD
Control 1.943±0.335
sh-hTERT#1 1.016±0.283
sh-hTERT#2 0.946±0.039
P < 0.05
D
HP1-β
Control
sh-hTERT#1
Relative fluorescent intensity
HeLa Mean±SD
Control 0.847±0.057
sh-hTERT#1 0.548±0.063
sh-hTERT#2 0.737±0.070
P < 0.05
E
MEF
mTERT(+/+) #1
mTERT(+/+) #2
mTERT(+/-) #1
mTERT(+/-) #2
mTERT(-/-) #1
mTERT(-/-) #2
RT-PCR
mTERT
β-actin
F
Relative expression
P < 0.05
mTERT
(+/+) #1
(+/+) #2
(-/-) #1
(-/-) #2
Sense
Antisense
IAP
mLINE1 Type A
mLINE1 Type Tf
G
Telomerase activity
RdRP activity
DMSO
β-rubromycin
nt
600
400
300
200
150
100
IC
I
ChIP
Control
Nocodazole
IgG
α-hTERT
Dot blot
TRF probe
Alu probe
Alphoid probe
hLINE1 probe
H
HeLa
VA13
DMSO
β-rubromycin
RT-PCR
Alphoid Sense
Alphoid Antisense
β-actin
Relative hLINE1 expression
P < 0.05
Sense
Antisense
J
Input (1%)
(-)
(+)
RNase I
IgG
α-hTERT
IP-RT-PCR
hTERC
RMRP
Alphoid
hLINE1 Sense
hLINE1 Antisense
RNase P

products. To confirm, we performed IP-RdRP assays using synthetic RNAs as templates (34 nt). Under such conditions, the chemically synthesized templates for the reaction are pure and highly homogeneous in size. Under these conditions, we also observed a smear and confirmed the production of intermediate-sized by-products of RdRP activity in this assay (Fig. 5C). To confirm that the template-sized products were double stranded, we used the sense strand of the *RMRP* as a probe in a Northern blot analysis of products from this assay. As expected, we detected the antisense strand of the template *RMRP* RNA from the cells synchronized in mitotic phase but not in the cells that contained the complex from asynchronously dividing cells (Fig. 5D). To further confirm that the products of the RdRP assay were dsRNAs, we treated the products with RNase V1, which digests dsRNA, and found that RNase V1 treatment eliminated all of these products (Fig. 5E). In addition, since we were unable to detect any RNA products in hTERT null VA13 cells even after treatment with nocodazole to arrest the cells in mitosis, we concluded that the products are generated in a TERT-dependent manner (Fig. 5F). Taken together, these observations confirm that hTERT isolated from cells arrested in mitosis acts as an RdRP to generate dsRNA.

Since suppression of hTERT affected *alphoid* transcript expression (Fig. 4A) and since hTERT binds *alphoid* transcripts (Fig. 4J), we tested whether *alphoid*-derived RNA served as a template for an *in vitro* IP-RdRP reaction by hTERT. We found that mixing hTERT immune complexes and *alphoid* RNA transcribed *in vitro* produced 171-nucleotide RNA products corresponding to the length of *alphoid* RNA (Fig. 6A). The products were resistant to RNase I treatment but sensitive to RNase V1 treatment (Fig. 6B). These results confirm that the products are dsRNAs.

RdRPs play a central role in the synthesis of dsRNAs that are processed into siRNAs. Since the hTERT and centromeric *alphoid* region produce double-stranded RNA in an *in vitro* assay, we monitored the existence of small RNAs (19 to 23 nt) from the cells treated with nocodazole or DMSO with probes corresponding to centromeric *alphoid* or *hLINE1* in Northern blotting. We found that these probes identified 20- to 23-nt RNAs in cells treated with nocodazole (Fig. 6C) and concluded that the RdRP activity mediated by hTERT produced small dsRNAs.

Argonaute (Ago) is essential for producing siRNAs and for heterochromatin maintenance in *S. pombe* (38), and an RdRP, Ago, Dicer, and nucleotidyltransferase are required for chromosome segregation in *C. elegans* (5, 6). We thus examined whether human AGO2 and Dicer were also essential for heterochromatin maintenance in human cells. Specifically, we examined whether suppression of human AGO2 or DICER1 affected heterochromatin formation at *alphoid* and *hLINE1* loci. We analyzed the *alphoid* and *hLINE1* RNA expression levels in cells in which we suppressed AGO2. We confirmed that RNAs from *alphoid* and *hLINE1* were upregulated in AGO2-depleted HeLa and MCF7 cells compared with levels in control cells, whereas suppression of AGO2 did not affect the RNA expression levels in VA13 cells (Fig. 6D and E). In contrast, when we suppressed DICER1, we failed to observe changes in *alphoid* and *hLINE1* expression (Fig. 6F and G). These results suggest that AGO2 but not DICER1 is essential for heterochromatin formation.

hTERT, BRG1, and NS form a functional complex during mitosis. Although hTERT-associated RdRP activity was enriched in mitosis, we failed to observe increased telomerase activity (RNA-dependent DNA polymerase activity) (Fig. 7A), as described previously (27). To investigate how the hTERT RdRP activity is regulated in mitosis, we tested whether increased levels of the TBN complex were found in mitosis. We first assessed the expression levels of each of the components of the TBN complex and noted that the levels of all three components were increased in mitosis (Fig. 7B). When we isolated ectopically expressed FLAG-hTERT, we found increased hTERT associated with BRG1 and NS in cells arrested in mitosis (Fig. 7C). Similarly, we also found that the interaction between endogenous TERT and NS was increased in mitosis (Fig. 7D).

When we investigated the subcellular location where hTERT and BRG1 interact during mitosis, we detected both TERT and BRG1 signals at spindles as marked with α-tubulin, a mitotic spindle marker (Fig. 7E, upper panel). Moreover, we found that hTERT and NS also colocalize at the mitotic spindle (Fig. 7E, lower panel). These observations suggest that increased amounts of the TBN complex are found at the mitotic spindle in mitosis.

To investigate whether manipulating the expression of the TBN complex affected mitosis, we suppressed BRG1 or NS with two independent shRNAs (Fig. 7F and G) (15) and assessed mitotic progression using $pHH3^{Ser10}$ (Fig. 7H) or DNA fluorescence intensity (Fig. 7I). We found an increase in the number of mitotic cells (2- to 5-fold) after suppression of either NS or BRG1 compared to cells expressing sh-*GFP* (all *P* values of <0.05) (Fig. 7H and I). The effect of suppressing NS and BRG1 was similar to what we observed in cells lacking hTERT (Fig. 2F and G). Together, these results demonstrate that the suppression of hTERT, BRG1, or NS has an inhibitory effect on mitotic progression.

We used sucrose density gradient centrifugation and an RdRP assay to examine the correlation between TBN complex formation and its RdRP activity during mitosis using cells treated with no-

FIG 4 Suppression of hTERT causes heterochromatin disassembly. (A) RT-PCR of *alphoid* and qRT-PCR of *hLINE1* RNA expression levels in HeLa cells expressing control and *hTERT*-specific shRNAs. β-Actin, internal control. *P* values for sh-*hTERT* 1 or sh-*hTERT* 2 versus sh-*GFP* were <0.05. (B) RT-PCR of *alphoid* or *hLINE1* RNA in hTERT-depleted MCF7 cells. RT(−), absence of RT; β-actin, internal control. (C) Effects of *hTERT* suppression on trimethylation of histone H3 lysine 9 (H3-K9). Cells expressing a control shRNA (sh-*GFP*) or two independent *hTERT*-specific shRNAs were stained with anti-trimethyl H3-K9 antibody. Green represents trimethylated H3-K9 staining, and red represents DAPI staining. (D) Effects of *hTERT* suppression on HP1-β expression. Cells expressing a control shRNA (sh-*GFP*) or two independent *hTERT*-specific shRNAs were stained with an anti-HP1-β antibody. Green represents HP1-β staining, and blue represents DAPI staining. (E) RT-PCR of *mTERT* expression levels in MEF cells derived from wild-type $mTERT^{+/+}$, heterozygous $mTERT^{+/-}$ or homozygous $mTERT^{-/-}$ mice. β-Actin, internal control. (F) qRT-PCR of *IAP*, *mLINE1 Type A* or *mLINE1 Type Tf* retrotransposons in MEF cells derived from wild-type $mTERT^{+/+}$ or homozygous $mTERT^{-/-}$ mice. β-Actin, internal control. *P* values for $mTERT^{-/-}$ versus $mTERT^{+/+}$ no. 1 were <0.05. (G) Inhibition of telomerase activity and RdRP activity in HeLa cells by β-rubromycin *in vitro*. RdRP activity was determined by IP-RdRP assay. β-Rubromycin at 15 μM and 10 μM was used for the TRAP assay and IP-RdRP assay, respectively. (H) RT-PCR of *alphoid* and qRT-PCR of *hLINE1* RNA expression levels in HeLa or VA13 cells treated with 20 μM β-rubromycin or DMSO (Control). β-Actin and GAPDH, internal controls. *P* values for β-rubromycin versus DMSO were <0.05. (I) ChIP performed in HeLa cells with or without (Control) nocodazole treatment using anti-hTERT MAb. Dot blot signals were detected with the indicated γ-^{32}P-labeled probes. (J) Detection of *hTERC*, *RMRP*, *alphoid* or *hLINE1* RNA by RT-PCR with (+) or without (−) RNase I treatment. RNA bound to hTERT was isolated from HeLa cells by IP and subjected to RT-PCR. Antisense-strand RNAs from *alphoid* were below detectable levels. RNase P, negative control.

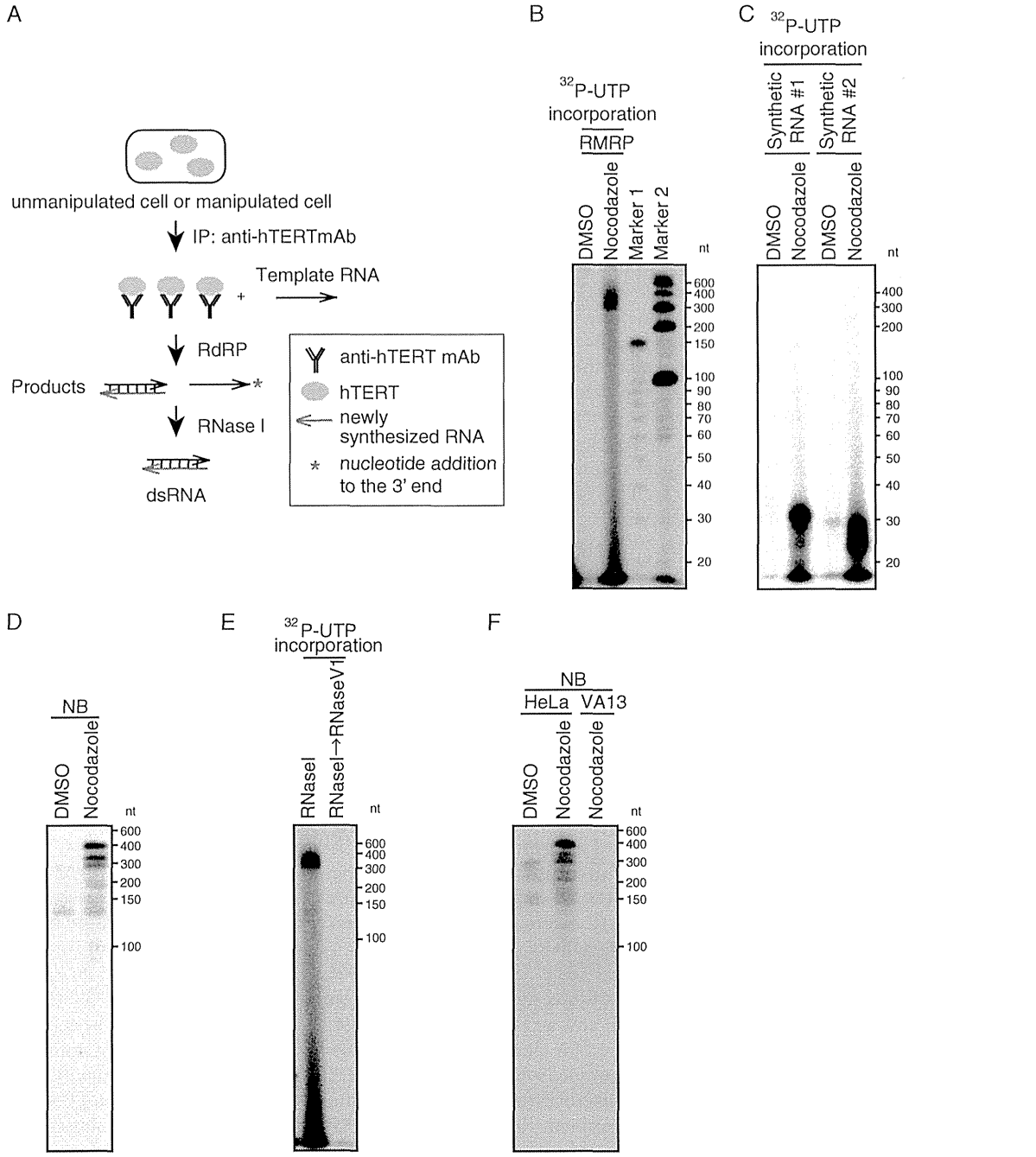

FIG 5 RdRP activity in mitotic cells. (A) Scheme of the IP-RdRP assay using cell lysate and anti-hTERT MAb. hTERT immune complexes were isolated by anti-hTERT MAb and then used for an RdRP assay with RNA templates. Double-stranded RNA was detected by UTP incorporation assay followed by RNase I treatment, or antisense RNA was detected by Northern blotting (NB). (B) IP-RdRP assay using cell lysates treated with nocodazole (manipulated) or DMSO (unmanipulated) and anti-hTERT MAb. *RMRP* was used as the RNA template. RdRP products were treated with RNase I. (C) IP-RdRP assay for HeLa cells treated with nocodazole or DMSO using synthetic RNAs (synthetic RNA 1 and synthetic RNA 2) as templates. The RNA products were analyzed with next-generation sequencing and confirmed to be intermediate-sized products complementary to the templates. (D) Northern blotting after an IP-RdRP assay using sense probe derived from nucleotides 229 to 267 of *RMRP*. (E) IP-RdRP assay using cell lysates treated with nocodazole with a combination of RNase I/RNase V1 or RNase I. (F) Northern blotting after an IP-RdRP assay using HeLa cells treated with nocodazole or DMSO or using VA13 cells treated with nocodazole. A sense probe derived from nucleotides 229 to 267 of *RMRP* was used. IP-RdRP products were treated with RNase I.

codazole or DMSO. Sucrose density gradient centrifugation was used to analyze the extracts. We confirmed that hTERT, BRG1, and NS were not coseparated in any fraction in unmanipulated cells, whereas these proteins were primarily found in fraction 10 in cells treated with nocodazole, which shows that synchronization shifts all three proteins into the upper fractions (Fig. 7J, left panels). To further investigate the possibility that the TBN complex serves as an RdRP, the BRG1 immune complex or NS immune complex was isolated from cells treated with nocodazole or DMSO, and an RdRP assay was performed (Fig. 7J). We found

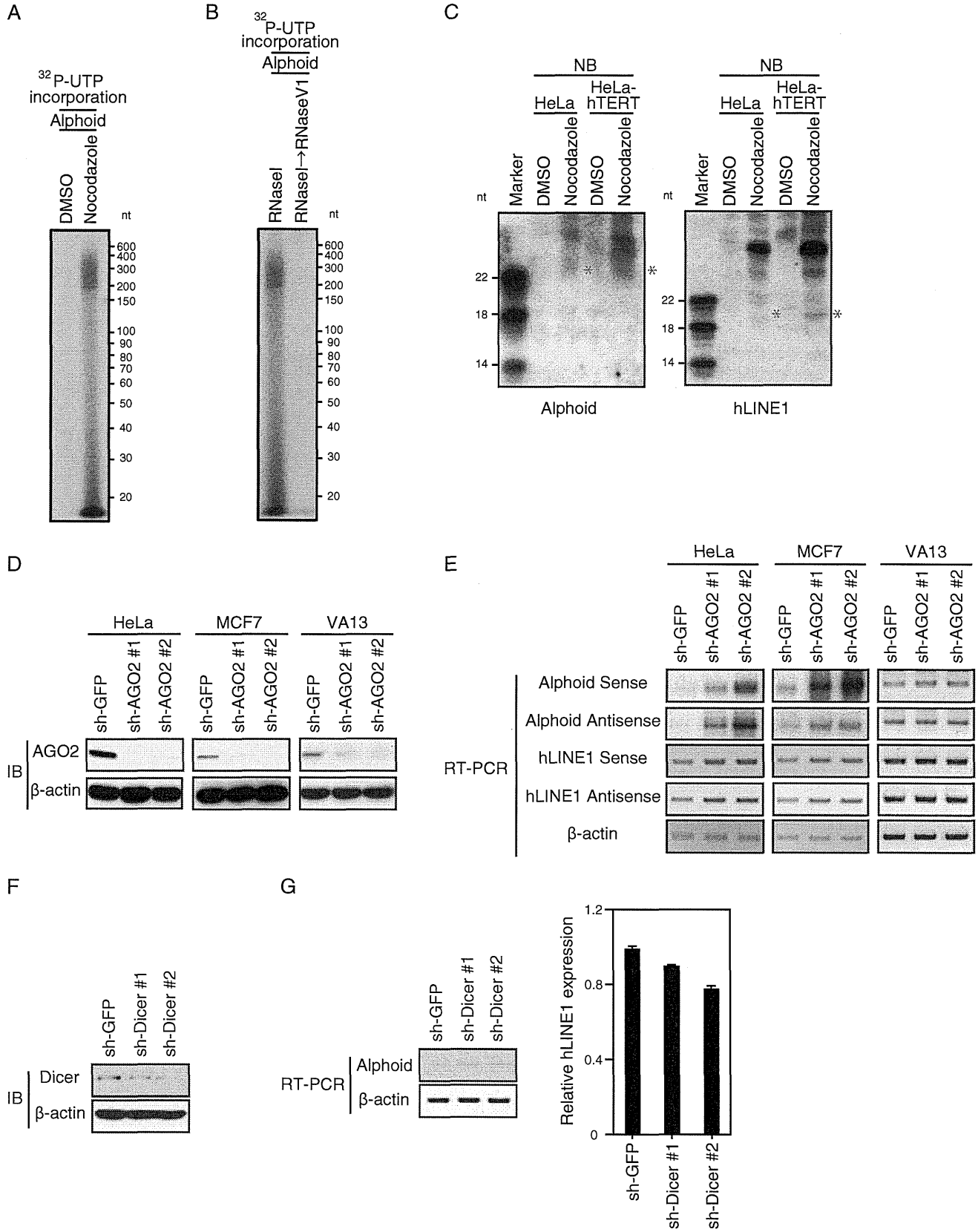

FIG 6 hTERT has a functional role in mitotic cells. (A) IP-RdRP assay using cell lysates treated with nocodazole (manipulated) or DMSO (unmanipulated) and anti-hTERT MAb. *alphoid* was used as the RNA template. (B) IP-RdRP assay using cell lysates treated with nocodazole with a combination of RNase I/RNase V1 or RNase I. *alphoid* was used as the RNA template. (C) Detection of small RNAs in cells treated with nocodazole or DMSO. Northern blotting (NB) to detect small RNAs using antisense probe derived from nucleotides 120 to 171 of *alphoid* or nucleotides 1 to 70 of *hLINE1*. Asterisks indicate the small RNAs detected by the antisense probes. (D) Immunoblot (IB) of AGO2 expression in HeLa, MCF7, or VA13 cells expressing control or *AGO2*-specific shRNAs. β-Actin, internal control. (E) RT-PCR of *alphoid* or *hLINE1* RNA expression levels in HeLa, MCF7, or VA13 cells expressing shRNAs. β-Actin, internal control. (F) IB of Dicer in Dicer-depleted HeLa cells. β-Actin, internal control. (G) RT-PCR of *alphoid* and qRT-PCR of *hLINE1* RNA expression levels in HeLa cells expressing control or *Dicer*-specific shRNAs. β-Actin, internal control.

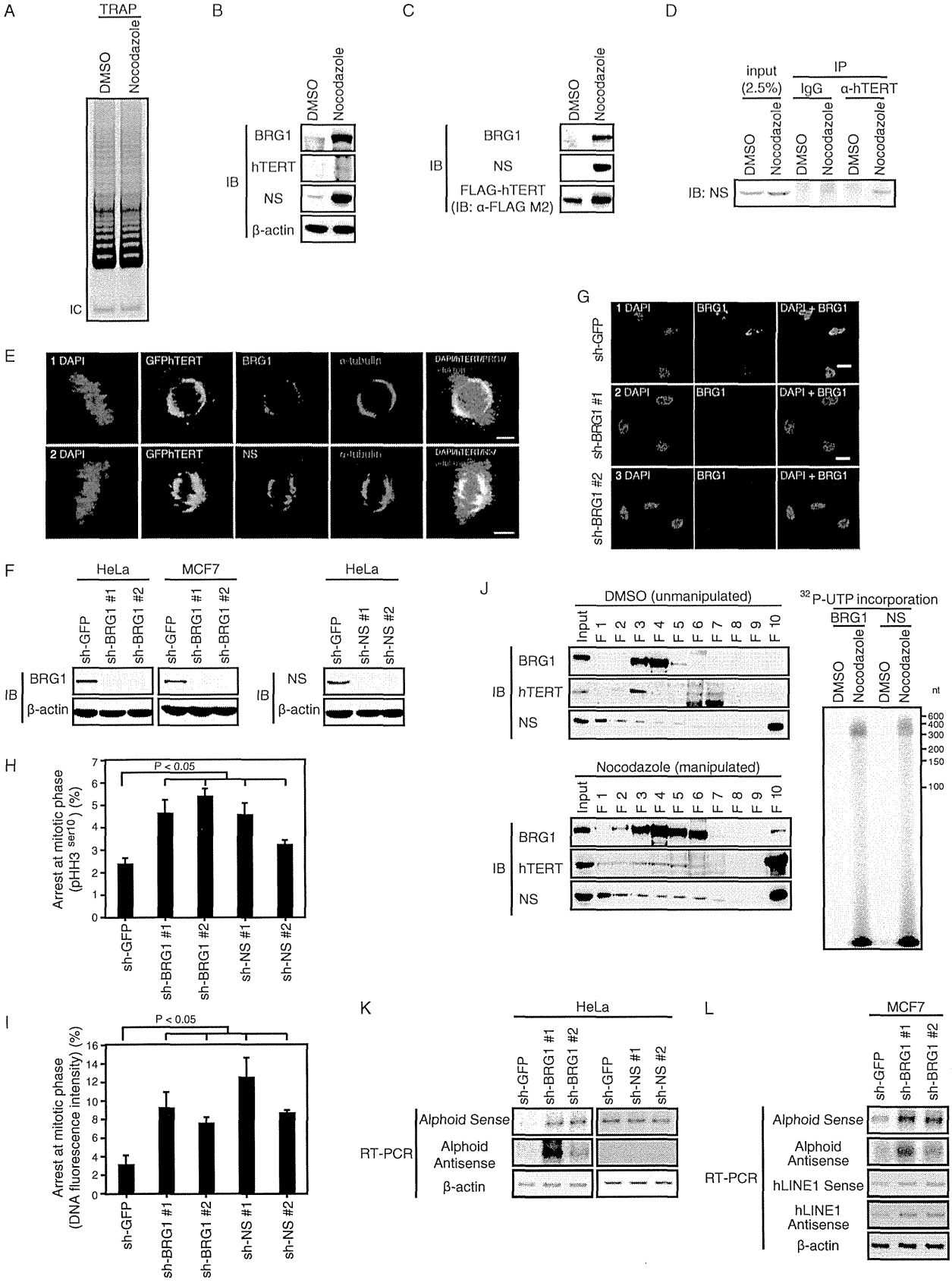
A
TRAP
DMSO
Nocodazole
IC
B
DMSO
Nocodazole
IB
BRG1
hTERT
NS
β-actin
C
DMSO
Nocodazole
IB
BRG1
NS
FLAG-hTERT
(IB: α-FLAG M2)
D
input
(2.5%)
IP
IgG
α-hTERT
DMSO
Nocodazole
IB: NS
E
1 DAPI
GFPhTERT
BRG1
α-tubulin
DAPI/hTERT/BRG1/
2 DAPI
GFPhTERT
NS
α-tubulin
DAPI/hTERT/NS/
G
sh-GFP
sh-BRG1 #1
sh-BRG1 #2
1 DAPI
2 DAPI
3 DAPI
BRG1
DAPI + BRG1
F
HeLa
MCF7
HeLa
sh-GFP
sh-BRG1 #1
sh-BRG1 #2
sh-NS #1
sh-NS #2
IB
BRG1
NS
β-actin
H
Arrest at mitotic phase
(pHH3 ser10) (%)
P < 0.05
sh-GFP
sh-BRG1 #1
sh-BRG1 #2
sh-NS #1
sh-NS #2
I
Arrest at mitotic phase
(DNA fluorescence intensity) (%)
P < 0.05
J
DMSO (unmanipulated)
Nocodazole (manipulated)
Input
F 1
F 2
F 3
F 4
F 5
F 6
F 7
F 8
F 9
F 10
IB
BRG1
hTERT
NS
32P-UTP incorporation
BRG1
NS
DMSO
Nocodazole
nt
600
400
300
200
150
100
K
HeLa
sh-GFP
sh-BRG1 #1
sh-BRG1 #2
sh-NS #1
sh-NS #2
RT-PCR
Alphoid Sense
Alphoid
Antisense
β-actin
L
MCF7
sh-GFP
sh-BRG1 #1
sh-BRG1 #2
RT-PCR
Alphoid Sense
Alphoid
Antisense
hLINE1 Sense
hLINE1
Antisense
β-actin

RdRP activity in both of the immune complexes isolated from cells treated with nocodazole (Fig. 7J), as observed with the hTERT immune complex (Fig. 5B). The results indicate that both BRG1 and NS are components of the hTERT RdRP complex.

To determine whether BRG1 and NS are essential for heterochromatin assembly, we examined the consequences of suppressing BRG1 and NS on heterochromatin formation at *alphoid* and *hLINE1* elements. Sense and antisense RNA strands from *alphoid* were upregulated in HeLa and MCF7 cells in which BRG1 was suppressed compared with cells expressing sh-*GFP* (Fig. 7K and L). However, suppression of NS did not affect *alphoid* RNA expression levels. These observations demonstrate that BRG1, but not NS, in addition to hTERT contributes to heterochromatin formation at *alphoid* and *hLINE1* loci. Together with the observation that hTERT, BRG1, and NS are all essential for heterochromatin maintenance and mitotic progression, we conclude that hTERT, BRG1, and NS form a functional complex which facilitates mitotic progression by regulating centromeric heterochromatin.

TBN and AGO2 interact in human cells. In *S. pombe*, Ago siRNA interacts with the RITS complex (2), raising the possibility that AGO2 interacts with the TBN complex in human cells. Since we found that expression of AGO2 is essential for heterochromatin formation at *alphoid* and *hLINE1* loci (Fig. 6D and E), we examined whether human AGO2 is associated with the TBN complex. Specifically, we assessed whether AGO2 binds NS or hTERT and found that endogenous AGO2 binds NS but not hTERT or BRG1 (Fig. 8A to C). To further characterize the interaction of AGO2 and NS, we used NS truncation mutants (15) and found that the amino-terminal region of NS was necessary for interactions with the endogenous AGO2 (Fig. 8D). Using IF, we further confirmed that, like the TBN complex, AGO2 localized to the mitotic spindles in HeLa cells during mitosis (Fig. 8E). These observations showed that AGO and NS interact and that AGO colocalizes to the TBN complex during mitosis. These results suggest that AGO2 is essential for heterochromatin formation by interaction with the TBN complex in mitosis.

DISCUSSION

Here, we show that the hTERT, BRG1, and NS complex assembles in mitosis and maintains heterochromatic repetitive elements, including those at centromeres and retrotransposons. Specifically, hTERT acting as an RdRP synthesizes dsRNA from nascent RNA from these regions, which is processed to siRNA that participates in the maintenance of heterochromatin at these same regions in a manner analogous to the RDRC complex in *S. pombe*. Suppressing the TBN complex disrupted heterochromatin formation at these loci and interrupted mitotic progression, suggesting that this complex participates in organizing chromatin during mitosis. Together, these observations indicate a non-telomere-directed function of hTERT in the regulation of heterochromatin.

The TBN complex. As telomerase, TERT localizes to telomeres and protects chromosome ends. In addition, several laboratories have demonstrated that TERT forms complexes independent of the telomerase RNA *hTERC* (9, 11, 15). Specifically, we along with others have found that hTERT binds BRG1 and NS and that this complex regulates both gene transcription (11) and stem cell function in normal and malignant cells (15, 39, 40) in a manner independent of telomere maintenance. Here, we report that the levels of this complex are increased in mitotic cells but not in asynchronously cycling cells (41) and that suppressing each of the members of this complex arrests cells in mitosis.

TERT levels and telomerase activity have been reported to be transiently upregulated in S phase, which leads to telomere stabilization (22, 27). Using a newly generated hTERT-specific antibody, we found that during M phase hTERT localizes to mitotic spindles and that suppression of each of the components of the TBN complex arrests cells in mitosis (Fig. 2F and G and 7H and I). We previously reported that cells expressing a dominant interfering hTERT mutant (DN-hTERT) or *hTERT*-specific shRNA accumulated in G_2/M phase (22) and exhibited slowed proliferation without telomere shortening. Suppression of hTERT or NS further induced a senescence-like phenotype in normal fibroblasts and cancer cells (15, 22). Although it remains unclear if the senescence-like proliferative arrest is related to hTERT function in M phase, these observations suggest that the distinct hTERT complexes act in different phases of the cell cycle.

We confirmed that hTERT localizes to both telomeres and Cajal bodies (Fig. 1E). In addition, we found that TERT associates with centromeres (Fig. 2D and E) and mitotic spindles (Fig. 2A to C) during mitosis. Prior work using GFP-hTERT fusion proteins showed that hTERT shuttles between subcellular compartments in both normal and malignant cells (42). We previously reported that telomerase activity is increased in S phase (22) and here confirmed that RdRP activity and the TBN complex are upregulated in mitosis. Together, these observations confirm and extend prior reports that hTERT is distributed among several complexes. Specifically, as telomerase, hTERT is shuttled between the nucleolus

FIG 7 hTERT, BRG1, and NS form a functional complex in mitotic cells. (A) Telomerase activity of HeLa cells with or without manipulation. Telomerase activity was detected by TRAP assay. IC, internal control. (B) Immunoblot (IB) using the indicated antibodies in HeLa cells treated with nocodazole or DMSO. β-Actin, internal control. (C) hTERT interacts with endogenous BRG1 and NS. FLAG-hTERT immune complexes in HeLa cells were precipitated with anti-FLAG M2 antibody and immunoblotted with anti-BRG1 and anti-NS antibody. (D) hTERT interacts with endogenous NS. hTERT immune complexes immunoprecipitated from HeLa cells and immunoblotted with anti-NS antibody. (E) BRG1 and NS colocalize with GFP-hTERT at mitotic spindles. HeLa-GFP-hTERT cells were immunostained with or without antibodies against BRG1, NS, and α-tubulin followed by DAPI staining. Scale bar, 5 μm. (F) IB of NS or BRG1 expression in HeLa or MCF7 cells expressing control, *BRG1*-specific shRNAs, or *NS*-specific shRNAs. β-Actin, internal control. (G) Immunofluorescence (IF) of BRG1 in HeLa cells. Suppression of BRG1 (sh-*GFP* as a control) was observed by IF. Representative images are shown. Scale bar, 20 μm. (H) A graph of the mitotic index according to $pHH3^{Ser10}$ immunofluorescence in HeLa cells expressing shRNAs. The *P* value for sh-*BRG1* or sh-*NS* versus sh-*GFP* was <0.05. (I) A graph of the mitotic index according to DNA fluorescence intensity and the morphology of HeLa cells expressing shRNAs. The *P* value for sh-*BRG1* or sh-*NS* versus sh-*GFP* was <0.05. (J) hTERT, BRG1, and NS form a complex with RdRP activity. Immunoblotting (IB) of fractionated cell lysates with or without manipulation (left panels) was performed. The lysates of HeLa-FLAG-hTERT cells treated with nocodazole (manipulated) or DMSO (unmanipulated) were fractionated into 10 fractions (F1 to F10) by sucrose density gradient centrifugation. The fractions were analyzed by IB with the indicated antibodies. IP-RdRP assay of HeLa cells using cell lysates treated with nocodazole or DMSO and anti-BRG1 or anti-NS antibody for IP (right panel) was performed. (K) RT-PCR of *alphoid* RNA expression levels in HeLa cells expressing control, *BRG1*-specific shRNAs, or *NS*-specific shRNAs. β-Actin, internal control. (L) RT-PCR of *alphoid* or *hLINE1* RNA in BRG1-depleted MCF7 cells. RT(−), absence of RT; β-actin, internal control.